



CHALMERS
UNIVERSITY OF TECHNOLOGY

Open-flask, ambient temperature direct arylation synthesis of mixed ionic-electronic conductors

Downloaded from: <https://research.chalmers.se>, 2025-06-04 07:57 UTC

Citation for the original published paper (version of record):

Kimpel, J., Kim, Y., Schomaker, H. et al (2025). Open-flask, ambient temperature direct arylation synthesis of mixed ionic-electronic conductors. *Science advances*, 11(19).
<http://dx.doi.org/10.1126/sciadv.adv8168>

N.B. When citing this work, cite the original published paper.

MATERIALS SCIENCE

Open-flask, ambient temperature direct arylation synthesis of mixed ionic-electronic conductors

Joost Kimpel^{1*}, Youngseok Kim¹, Hannes Schomaker², Diego R. Hinojosa³, Jesika Asatryan⁴, Jaime Martín⁴, Renee Kroon^{5,6}, Michael Sommer³, Christian Müller^{1,7,8,9*}

Conjugated polymers are widely studied for application areas ranging from energy technology to wearable electronics and bioelectronics. To develop a truly sustainable technology, environmentally benign synthesis is essential. Here, the open-flask synthesis of a multitude of conjugated polymers at room temperature by ambient direct arylation polymerization (ADAP) is demonstrated. The batch synthesis of over 100 grams of polymer in a green solvent and continuous droplet flow synthesis without any solid support is described. Polymers prepared by ADAP are characterized by improved structural order compared to materials prepared by other methods. Hence, organic electrochemical transistors (OECTs) feature beyond state-of-the-art electrical properties, i.e., an OECT hole mobility μ as high as $6 \text{ cm}^2 \text{ V}^{-1} \text{ s}^{-1}$, a volumetric capacitance C^* over 200 F cm^{-3} , and thus a figure of merit [μC^*] exceeding $1100 \text{ F cm}^{-1} \text{ V}^{-1} \text{ s}^{-1}$. Thus, ADAP paves the way for the benign and large-scale production of high-performance conjugated polymers.

INTRODUCTION

Conjugated polymers receive widespread interest for a myriad of applications from energy technology to wearable electronics and bioelectronics (1–5). To become truly viable, organic electronics must have a minimal environmental footprint that necessitates green synthesis and production (6–8). Materials should be selected not only for their superior electrical properties, but also for their accessibility via synthetic routes with low environmental impact. Several metrics are used to judge the environmental impact of a material. Those include (i) the synthetic complexity index (SCI) (9), which is a parameter that summarizes the number of synthetic steps, yield, workup procedures, and hazards involved; (ii) the environmental factor (E-factor) (10), which corresponds to the ratio of waste to product; and (iii) the reaction mass efficiency (11), composed of the fraction of atoms that are converted from starting material to the desired product. In addition, the energy required to sustain the polymerization must be considered, i.e., the heat supplied and its duration. Accordingly, the synthesis of a promising conjugated polymer should be associated with a low SCI, E-factor, and energy/time requirement, and have a high reaction mass efficiency.

The vast majority of conjugated polymers are synthesized by cross-coupling reactions between two bifunctional monomers. The most common cross-coupling polycondensations include Stille coupling, Suzuki coupling, and Kumada coupling, all of which require two functional groups. The required monomer functionalization not only

adds a synthetic step but also yields toxic organotin monomers (Stille), heavy organoboron compounds (Suzuki), or reactive organometallic Grignard intermediates generated in situ (Kumada). An alternative is direct arylation polymerization (DAP) that involves cross-coupling of reactive aromatic C–H bonds with aryl halides, which constitutes a substantial advantage compared with other cross-coupling reactions in terms of SCI and E-factors. However, DAP requires bulky acid and inorganic base additives and is prone to side reactions such as homo-coupling (self-condensation of monomers) (12, 13), causing a stoichiometric imbalance if homocoupling differs between monomers (14), and β defects (reaction of wrong carbon-hydrogen bond) (15), leading to branching, cross-conjugation, steric crowding, and cross-linking. The ensuing structural disorder tends to result in uncontrolled opto-electronic properties (16, 17). Moreover, it has proven to be difficult to achieve appreciable degrees of polymerization (18). While there are some examples of high molar mass materials free of defects, these require monomers with distinct structural motifs that have gone through extensive optimization studies, which therefore do not serve as universal protocols (19–21).

Many studies have attempted to use DAP for the synthesis of organic mixed ionic-electronic conductors (OMIECs), which are promising for energy harvesting and storage devices (22) and constitute the champion materials for bioelectronic devices such as organic electrochemical transistors (OECTs) (23). Promising monomers for DAP to OMIECs include 3,4-ethylenedioxythiophene (EDOT) (24, 25), 3,4-bis(triethylene glycol monomethyl ether)thiophene (26), and 3,6-bis(triethylene glycol monomethyl ether)thieno[3,2-*b*]thiophene ($g_3\text{TT}$) (26), which only feature two active C–H bonds and thus cannot suffer from β -arylation. Recently, DAP involving these monomers, which used an Ozawa-derived catalytic system, has been used for the synthesis of OMIECs such as $p(g_3\text{TT-T2})$ (see Fig. 1 for chemical structure) with a number-average molecular weight $M_n > 10 \text{ kg mol}^{-1}$ and an OECT mobility μ of up to $2 \text{ cm}^2 \text{ V}^{-1} \text{ s}^{-1}$ (27). In comparison, one of the most widely used OMIECs, synthesized by Stille cross coupling, is $p(g_3\text{T2-TT})$ (fig. S1), which features an OECT mobility of $\mu = 1.3 \text{ cm}^2 \text{ V}^{-1} \text{ s}^{-1}$ (23, 28). Through removal of the palladium catalyst from the polymer $p(g_4\text{T2-TT})$ (fig. S1) by preparative high-pressure liquid chromatography (prep-HPLC), OECT mobilities of up to $\mu =$

¹Department of Chemistry and Chemical Engineering, Chalmers University of Technology, Göteborg, Sweden. ²AutoSyn AB, Hisings Backa, Göteborg, Sweden. ³Institut für Chemie & Forschungszentrum MAIN, Technische Universität Chemnitz, Chemnitz, Germany. ⁴Universidade da Coruña, Campus Industrial de Ferrol, CITENI, Esteiro, Ferrol, Spain. ⁵Laboratory of Organic Electronics, Department of Science and Technology, Linköping University, Norrköping, Sweden. ⁶Wallenberg Initiative Materials Science for Sustainability, Department of Science and Technology, Linköping University, Norrköping, Sweden. ⁷Wallenberg Initiative Materials Science for Sustainability, Department of Chemistry and Chemical Engineering, Chalmers University of Technology, Göteborg, Sweden. ⁸Wallenberg Wood Science Center, Department of Chemistry and Chemical Engineering, Chalmers University of Technology, Göteborg, Sweden. ⁹Stellenbosch Institute for Advanced Study, Wallenberg Research Centre at Stellenbosch University, Stellenbosch, South Africa.

*Corresponding author. Email: kimpel@chalmers.se (J.K.); christian.muller@chalmers.se (C.M.)

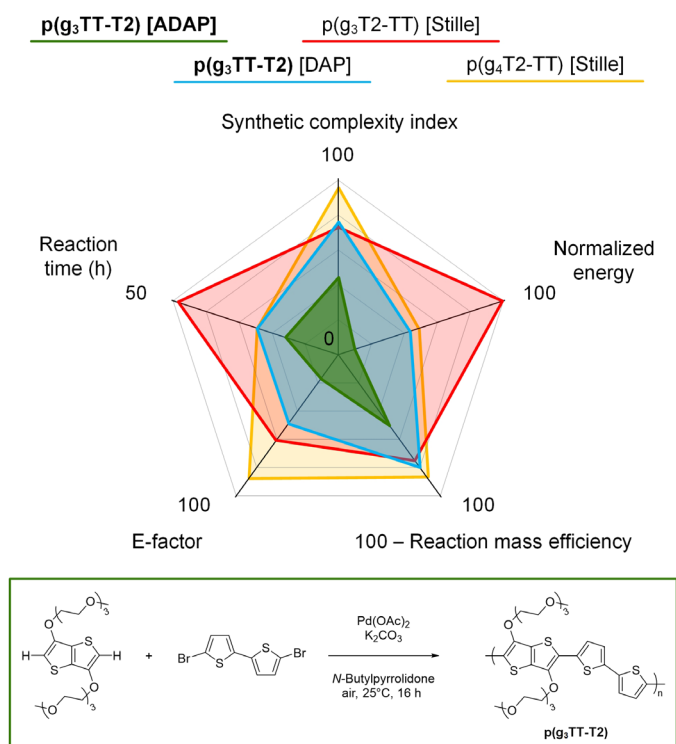


Fig. 1. Environmental impact comparison of different conjugated polymers. Radar plot comparing the environmental impact of the synthesis of conjugated polymers with oligoether side chains; lower numbers indicate a greener and more sustainable synthesis. All environmental impact factors in this plot are calculated for the polymerization step only (SCI_{poly} for the synthetic complexity index). Note that syntheses as described in the literature were considered (27–29), which were not optimized for the factors discussed here. Polymer structures, polymerization conditions, definitions, and derivations are found in section S1.

$8.5 \text{ cm}^2 \text{ V}^{-1} \text{ s}^{-1}$ could be achieved (29). While promising, upscaling would be complex since prep-HPLC has limited sample loading and polymers often contaminate the column material. Despite the avoidance of stannylated monomers for $p(g_3TT-T_2)$ made via DAP, its polymerization step is associated with a relatively high SCI and E-factor compared to the Stille-synthesized polymers. Evidently, while DAP has many advantages, its use alone is no guarantee for a significantly greener production of conjugated polymers.

Although elevated temperatures are typically selected, copolymerization methods have recently been found to proceed at room temperature under specific conditions. This has been achieved through, e.g., the design of a specific catalytic system (Stille) (30), employment of a highly nucleophilic base (Suzuki) (31), or increased monomer concentration (Kumada) (32). Instead, universal room temperature DAP has been more difficult to realize, while reactions both at room temperature and in air have not yet been explored. Only oligomeric compounds have been obtained at room temperature under inert conditions in specific cases through the addition of stoichiometric amounts of silver oxide and nitrobenzoic acid to an iodoarene (33), or by using a diiodinated comonomer (34).

Stille, Suzuki and Kumada cross-coupling reactions benefit from easier translation to large batch synthesis or flow synthesis, which are needed for upscaling and large-scale production. For example, Xiong *et al.* have recently demonstrated that Suzuki-Miyaura

polymerization of a wide range of materials can be carried out at room temperature and facilitates batch synthesis of up to 100 g of a fluorene-thiophene copolymer (31). Flow synthesis of conjugated polymers has been achieved with Stille-based (35), Suzuki-based (35), and Kumada-based reactions (36). Flow synthesis allows for better reproducibility once steady-state conditions are reached, i.e., the preparation of materials with more consistent property portfolios (37). The lack of wider implementation of flow synthesis for conjugated polymers is due to reactor fouling in traditional flow reactors, which can be overcome by creating reaction droplets inside a carrier fluid (38–40). One drawback to this method is that the most widely used carrier fluid is a perfluorinated alkyl substance (PFAS), a “forever chemical” (41).

Flow synthesis processes that involve DAP have been difficult to implement (42, 43). A base-loaded solid-phase reactor was required to avoid the blockage of valves by poorly soluble inorganic bases, which cannot be used in a steady-state flow system and requires excessive cleaning because of fouling. Evidently, a process that proceeds rapidly, allowing either a fast or room temperature reaction (low energy requirement), that offers a high yield (low SCI, low E-factor, and high reaction mass efficiency), and that is compatible with flow synthesis would significantly expand the efficacy and reach of DAP for the production of conjugated polymers.

Here, we show that rapid DAP of a wide range of OMIEC monomer combinations can be achieved by using a bimetallic Pd^{II}/Pd^0 catalytic system, initiated by the partial in situ reduction of an air-stable Pd^{II} catalyst to facilitate the presence of both Pd^{II} and Pd^0 species in the reaction. The reaction readily proceeds at room temperature and in air without the need of an acid additive. The polymerization can be carried out in the green solvent *N*-butyl-2-pyrrolidone (NBP) (44). In combination with a high yield of more than 90% after workup, this results in a favorable energy requirement, E-factor, reaction mass efficiency, and SCI of the polymerization step (SCI_{poly}) compared to other cross-coupling reactions that yield similar polymers, which have been previously synthesized (Fig. 1, figs. S1 to S5, and tables S1 to S5) (27–29). We note that the previously reported polymerizations have not been directly optimized for these factors.

The introduced open-flask, ambient DAP (ADAP) process allows for the preparation of a wide range of OMIEC materials that feature high yields and an $M_n > 10 \text{ kg mol}^{-1}$ [determined by nuclear magnetic resonance (NMR) end-group analysis and size exclusion chromatography (SEC)]. A thorough study of the mechanism indicates that the reaction at ambient conditions proceeds owing to homocoupling of the H-source monomer, which facilitates a bimetallic Pd^{II}/Pd^0 catalytic system. Exemplar $p(g_3TT-T_2)$ made by this method has a high OECT mobility of up to $6 \text{ cm}^2 \text{ V}^{-1} \text{ s}^{-1}$, which exceeds the performance of state-of-the-art OMIEC materials. We show that the high mobility arises because homocoupling, which initiates ADAP, improves the degree of order of the resulting polymers. ADAP is also used to synthesize fluorinated conjugated polymers, which subsequently can be modified post-polymerization, creating the possibility of equipping room temperature synthesized conjugated polymers with a wide variety of functionalities. To demonstrate the versatility of ADAP, a 100-g batch is prepared with an open-flask reaction at room temperature. Moreover, ADAP allows for the translation to continuous flow without the use of “forever chemicals” and without the requirement of a solid support—a first of its kind for DAP. Together, this suggests that benign production processes of OMIEC materials are now within reach.

RESULTS

In a first set of experiments, we carried out reactions of g_3TT and Br-T2-Br using a Fagnou-derived catalytic system (45), i.e., the Pd^{II} catalyst Pd(OAc)₂ in combination with potassium carbonate, and pivalic acid in *N,N*-dimethylacetamide (DMA) at various temperatures under inert conditions. Castillo and Thompson have recently reported the preparation of typically low molecular weight polymers via DAP at room temperature under inert conditions using similar conditions (34). At 110°C, a deep purple solid formed from the initial yellow solution within minutes, which was insoluble in chloroform, chlorobenzene, and *o*-dichlorobenzene due to cross-linking via the β C–H on Br-T2-Br. At room temperature, ADAP readily initiated but proceeded more slowly and was hence only terminated after 24 hours. Immediate initiation of the ADAP reaction between g_3TT and Br-T2-Br was indicated by an almost instantaneous change in color of the solution from clear yellow to turbid orange upon addition of the catalyst, followed by a gradual transition to red, burgundy, magenta, purple, and ultimately dark purple. Reaction progress was monitored by visual inspection of the color as well as precipitation of aliquots of the reaction mixture in *n*-hexanes, ethyl acetate, and chloroform (fig. S6).

To identify a suitable set of ADAP reaction conditions, we performed a series of polymerizations in DMA with a monomer concentration $[M]_0 = 50$ or 100 mM, catalyst loading $n_{cat} = 2$ or 5 mol %, reaction temperature $T = 25^\circ$ or 40°C , and the presence or absence of pivalic acid under inert or ambient atmosphere (Table 1). A lower concentration, lower catalyst loading, and lower reaction temperature led to an increase in reaction time that was required to obtain a chloroform-soluble polymer fraction with a yield of at least 60% after workup. The reaction time was unaffected by the presence or absence of pivalic acid and the reaction atmosphere. We deemed a longer reaction time beneficial because this allowed us to carefully

select the point at which the reaction was to be quenched by precipitation in hexane. For example, a polymer batch with a high yield of 92% after workup was obtained when carrying out the polymerization at $T = 25^\circ\text{C}$ in air for $t = 24$ hours ($[M]_0 = 100$ mM, $n_{cat} = 2$ mol %, no pivalic acid; Table 1, entry 7). This polymer batch featured a number-average molecular weight $M_{n,NMR} = 18$ kg mol⁻¹, determined by NMR end-group analysis as described for p(g_3TT -T2) in a previous study (27).

Hong and colleagues have proposed that direct arylation of small molecules with a Pd^{II} catalyst in the presence or absence of a phosphine ligand proceeds via a bimetallic Pd^{II}/Pd⁰ catalytic system (46). Inspired by this work, we set out with the hypothesis that the ADAP reaction between g_3TT and Br-T2-Br can occur in the presence of Pd(OAc)₂ owing to the in situ formation of Pd⁰ and a subsequent Pd^{II}/Pd⁰ system. This requires an initiation cycle during which g_3TT coordinates to Pd^{II} followed by transmetalation with another Pd^{II} center holding a second g_3TT . Subsequent reductive elimination results in a homocoupled product, in agreement with Kuwabara *et al.* who have shown that phosphine-free DAP in the presence of a Pd^{II} catalyst results in significant homocoupling of the H-source monomer (47). Oxidative addition of the aryl bromide to the in situ formed Pd⁰ takes place, after which the H-source monomer transmetalates onto the same Pd^{II} core. The cross-coupling is completed by reductive elimination (see Fig. 2A for schematic). Owing to the change in reaction mechanism from DAP, and accordingly the rate-determining step from concerted metalation-deprotonation to transmetalation, the ADAP reaction is allowed to proceed at room temperature (48). We would like to point out, however, that ADAP gives rise to a lower M_n and greater amount of homocoupling compared to DAP (see Table 1).

We carried out a number of model experiments to confirm that ADAP of g_3TT and Br-T2-Br in the presence of Pd(OAc)₂ follows the

Table 1. Synthesis of p(g_3TT -T2). Monomer concentration $[M]_0$; Pd catalyst loading n_{cat} ; presence of pivalic acid; reaction solvent, atmosphere, temperature T , and time t ; yield of highest molecular weight fraction from Soxhlet extraction relative to the loading of monomers; number-average molecular weight from SEC and NMR, $M_{n,SEC}$ and $M_{n,NMR}$; polydispersity index (PDI) from SEC; concentration of homocouplings n_{homo} from NMR spectra recorded at 120°C in $\text{C}_2\text{D}_2\text{Cl}_4$ (figs. S17 to S42 and tables S8 to S11); the preparation of polymer no. 1 by DAP has been described previously (27). RBF, round-bottom flask; EF, Erlenmeyer flask; B, beaker.

No.	Synthetic method	$[M]_0$ (mM)	Catalyst	n_{cat} (mol %)	Acid	Solvent	Atmosphere	T (°)	t (hours)	Yield (%)	$M_{n,SEC}$ (kg mol ⁻¹)	PDI	$M_{n,NMR}$ (kg mol ⁻¹)	n_{homo} (%)
1	Batch	50	Pd ₂ dba ₃ ·CHCl ₃	3	✓	Toluene	Inert	110	3	28	29	2.1	39	0.2
2	Batch	50	Pd(OAc) ₂	5	✓	DMAc	Inert	40	4	60	15	3.0	12	4.5
3	Batch	50	Pd(OAc) ₂	2	✓	DMAc	Inert	40	12	63	20	2.0	19	2.1
4	Batch	50	Pd(OAc) ₂	5	✓	DMAc	Inert	25	16	91	26	2.3	9	3.6
5	Batch	100	Pd(OAc) ₂	2	✓	DMAc	Inert	25	24	67	10	2.1	12	2.0
6	Batch	100	Pd(OAc) ₂	5	×	DMAc	Air	25	8	87	24	2.1	19	3.1
7	Batch	100	Pd(OAc) ₂	2	×	DMAc	Air	25	24	92	33	2.0	18	2.2
8	Batch	100	Pd(OAc) ₂	5	×	NBP	Air	40	12	81	15	2.5	11	6.6
9	Batch	100	Pd(OAc) ₂	5	×	NBP	Air	25	16	97	19	2.9	14	3.2
10	Batch, 1 g, RBF	100	Pd(OAc) ₂	5	×	NBP	Air	25	16	65	13	1.5	9	2.9
11	Batch, 1 g, EF	100	Pd(OAc) ₂	5	×	NBP	Air	25	16	54	15	1.8	9	1.6
12	Batch, 1 g, B	100	Pd(OAc) ₂	5	×	NBP	Air	25	16	45	7	2.7	4	3.8
13	Batch, 100 g, RBF	100	Pd(OAc) ₂	5	×	NBP	Air	25	30	76	9	1.8	11	1.6
14	Flow 10 repeats	37.5	Pd(OAc) ₂	5	×	NMP/ H ₂ O	Inert	100	0.3	≈100	13	1.4	11 ± 1	1.5 ± 0.8

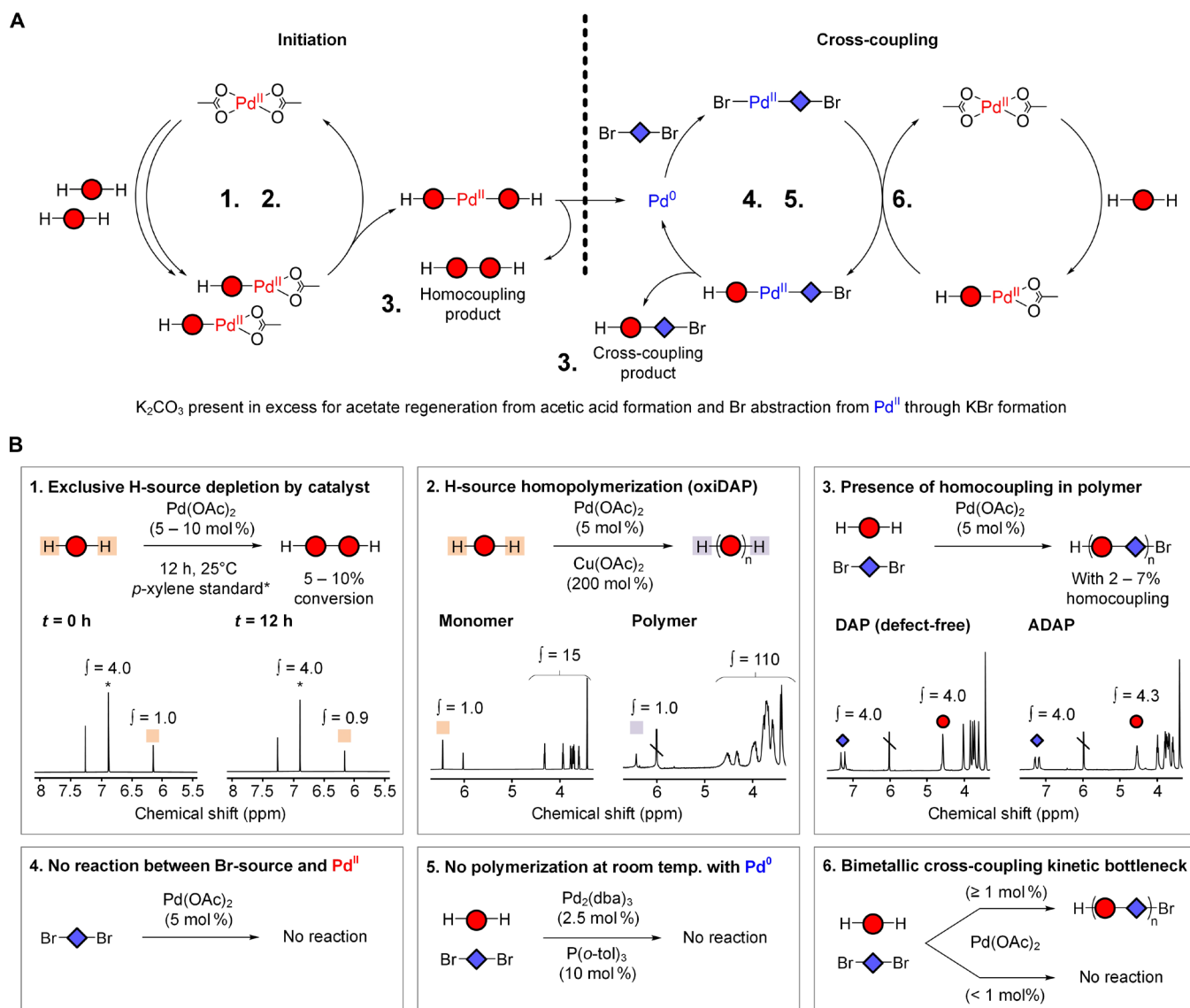


Fig. 2. ADAP mechanism. (A) Proposed mechanism for ADAP. (B) Performed model reactions: (1) reaction between H-source monomer and catalyst with NMR spectra indicating partial conversion; (2) oxidative DAP between H-source monomer and catalyst in the presence of an oxidant with NMR spectra showcasing homopolymer formation; (3) ADAP polymerization; NMR spectra of polymers prepared by DAP and ADAP show prevalence of homocoupling in case of the latter; (4) lack of reaction between aryl bromide and catalyst; (5) lack of ADAP when using a Pd^0 catalyst; (6) readiness of reaction with differing catalyst concentrations.

proposed bimetallic $\text{Pd}^{\text{II}}/\text{Pd}^0$ catalytic system. First, the tendency of homocoupling of the H-source, g_3TT , is evaluated by performing a reaction involving g_3TT , $\text{Pd}(\text{OAc})_2$, and potassium carbonate in DMA, i.e., the aryl bromide is absent and hence no cross-coupling reaction can occur. The depletion of g_3TT in the presence of various catalyst loadings was confirmed by NMR by comparing the aromatic g_3TT signal at 6.16 ppm with the 6.90 ppm signal from a *p*-xylene internal standard as the reaction progressed (Fig. 2B1 and fig. S7). The formation of homocoupled product was also validated by liquid chromatography–mass spectrometry (LC-MS; figs. S8 and S9). NMR and LC-MS indicate that the conversion is between 4% (low catalyst loading) and 10% (high catalyst loading). To further substantiate the occurrence of the homocoupling initiation cycle and whether it could continually persist, giving rise to homopolymerization of g_3TT , copper(II) acetate

monohydrate was added as an oxidant to investigate if oxidative DAP can be performed (49). A red-brown viscous compound could be obtained at a reaction temperature of 100°C, which was characterized with high-temperature NMR. A significantly higher triethylene glycol chain content per aromatic content compared to $\text{p}(\text{g}_3\text{TT}-\text{T}2)$ was deduced, which confirmed that homopolymerization of g_3TT had occurred (Fig. 2B2 and fig. S10). Another indicator of homocoupling was observed by high-temperature NMR measurements of the $\text{p}(\text{g}_3\text{TT}-\text{T}2)$ copolymer formed by ADAP in the presence of $\text{Pd}(\text{OAc})_2$. We compared the recorded NMR spectra with those of homocoupling-free $\text{p}(\text{g}_3\text{TT}-\text{T}2)$ made using an Ozawa-derived catalytic system (Pd^0) (27). The integral of the signal at 4.56 ppm, assigned to the first CH_2 of the triethylene glycol side chains of g_3TT , was found to increase by approximately 2 to 7% relative to the signals arising from T2 at 7.25 ppm

(Fig. 2B3 and Table 1). This agrees with the number of homocoupling reactions observed for g_3 TT in the absence of Br-T2-Br (Fig. 2B1). The homocoupling was also confirmed with matrix-assisted laser desorption/ionization–time of flight (MALDI-TOF) spectrometry (fig. S11), despite the fragmentation that likely occurred (50). Homocoupling has been observed by Reynolds and co-workers for biEDOT copolymers synthesized at 140°C (51).

The possibility of homocoupling of Br-T2-Br could be ruled out by carrying out the same reaction in the absence of g_3 TT (Fig. 2B4). The lack of any reaction also indicated that crosslinking of the β C–H on Br-T2-Br is highly unlikely under ADAP conditions. The necessity of the bimetallic Pd^{II}/Pd⁰ catalytic system was in line with the absence of any reaction at room temperature when a Pd⁰ catalytic system, i.e., Ozawa-derived conditions, was used instead (Fig. 2B5). No change in color was observed, and neither was any monomer converted as indicated by NMR. Moreover, no reaction occurred when varying (i) the Pd⁰ catalyst, i.e., tris(dibenzylideneacetone)dipalladium (0) or tetrakis(triphenylphosphine)palladium (0), (ii) the phosphine ligand, i.e., tri(*o*-tolyl)phosphine or tri(*o*-anisyl)phosphine, (iii) the base, i.e., cesium carbonate and potassium carbonate, and (iv) the solvent, i.e., toluene, DMA, or chlorobenzene.

Hong and Kim found that in case of a bimetallic Pd^{II}/Pd⁰ catalytic system, a kinetic bottleneck arises once the catalyst concentration falls below commonly used 2 to 5 mol % (48). The first-order dependence on catalyst concentration is substituted for a second-order dependence at very low palladium concentrations (below ~1 mol %), corroborating the transmetalation step between palladium centers. In case of Pd(OAc)₂ without ligands, second-order behavior was observed for palladium concentrations of 0.25 to 0.75 mol % (46). Note that at these concentrations, between 0.03 and 0.3% reagent conversion was observed in 1 hour as opposed to over 50% reagent conversion at 3 mol % catalyst loading. We evaluated the prevalence of this bimetallic system bottleneck for ADAP of g_3 TT and Br-T2-Br in the presence of Pd(OAc)₂ by changing the catalyst concentration from 5 mol % down to 0.1 mol %. After 24 hours at room temperature, the color changed to red, magenta, or dark purple for 1 to 5 mol %. Instead, the color of the solution did not vary for 0.5 and 0.1 mol % Pd(OAc)₂, and NMR only indicated limited conversion (<1%) of g_3 TT for the same catalyst concentrations. No consumption of Br-T2-Br was observed for the latter two reactions (Fig. 2B6 and fig. S12). The occurrence of a Pd^{II}/Pd⁰ bimetallic system was substantiated by (partial) reduction of Pd^{II} to Pd⁰ before the start of the polymerization reaction at room temperature. Pd(OAc)₂ was mixed with varying amounts of triphenylphosphine in inert atmosphere to create Pd⁰ species before addition to the reaction. Despite the addition of small amounts of triphenylphosphine (≤ 10 mol %) to the Pd(OAc)₂ catalyst, the ADAP reaction proceeded at a similar speed judging by the rate of color change, but slowed down significantly or was inhibited when larger amounts were used (15 mol % or more than 20 mol %; fig. S13).

DMA is a common solvent for DAP in the presence of Pd(OAc)₂ (52). Pd(OAc)₂, which coexists as a monomeric and oligomeric species, has an increased content of the former in amides owing to the lack of ligation to metal centers while still possessing a large dipole (53). We were interested in replacing DMA with a more benign solvent that would ease upscaling of ADAP and opted for NBP, which is classified as a “green solvent” (44). Besides the common DAP solvents tetrahydrofuran and toluene, we also explored green solvents that

have been used previously for DAP such as 2-methyltetrahydrofuran, cyclopentyl methyl ether, and anisole (54, 55) as well as the green solvent propylene carbonate. We observed that ADAP of g_3 TT and Br-T2-Br only proceeded in all these non–amide-based solvents once 20% (v/v) DMA was added, confirming the need for an amide-based solvent. NBP was also a good candidate since it easily solubilized p(g_3 TT-T2) upon heating, at around 50 g liter⁻¹, much higher than other amide solvents (between 1 and 20 g liter⁻¹), which can be anticipated to prevent precipitation during polymerization. The speed of ADAP in different amide solvents including DMA, NBP, as well as formamide, *N,N*-dimethylformamide (DMF), 2-pyrrolidone (NHP), and *N*-methyl-2-pyrrolidone (NMP) was examined (fig. S14). To this end, we monitored ADAP of g_3 TT and Br-T2-Br in the presence of Pd(OAc)₂ over the course of 24 hours in deuterated dimethylformamide (DMF-d₇) as well as mixtures of DMF-d₇ with formamide, DMA, NHP, NMP, or NBP (Fig. 3A). NMR tubes were charged with reagents, and frequent NMR spectra were recorded. The conversion was defined according to the decreasing aromatic peak from g_3 TT at 6.79 ppm with respect to the DMF-d₇ peak at 8.03 ppm. ADAP in formamide and NHP suffered from solubility issues and did not initiate, possibly owing to N–H hydrogen bond interactions between solvent molecules. Instead, ADAP proceeded at a comparable rate in both DMF-d₇ and DMF-d₇:DMA, as evidenced by the similar evolution of the conversion with time, and proceeded at a slower speed in DMF-d₇:NMP and DMF-d₇:NBP (Fig. 3A). Accordingly, the initial rates of g_3 TT depletion were 9.84 μ M s⁻¹ in DMF, 9.85 μ M s⁻¹ in DMA, 6.81 μ M s⁻¹ in NMP, and 5.34 μ M s⁻¹ in NBP, which correlate with Reichardt’s solvent polarity scale (Fig. 3B), indicating that the reaction kinetics depend on the polarity of the solvent. Evidently, ADAP of g_3 TT and Br-T2-Br in the presence of Pd(OAc)₂ readily proceeds in NBP at room temperature, albeit at a slightly lower rate due to the lower polarity of the solvent compared to other amide solvents.

We used the conditions deemed optimal for ADAP of g_3 TT and Br-T2-Br in DMA ($[M]_0 = 100$ mM, $n_{\text{cat}} = 5$ mol %, no pivalic acid, $T = 25^\circ\text{C}$, air) but instead used NBP as the reaction solvent, which resulted in a soluble polymer fraction with an $M_{n,\text{NMR}} = 14$ kg mol⁻¹ and a high yield of 97% after workup (Table 1, entry 9). We used Carothers equation to calculate the expected degree of polymerization DP

$$\text{DP} = \frac{1+r}{1+r-2rp} \quad (1)$$

where r is the stoichiometric ratio of the two monomers and p is the conversion. A typical ADAP prepared p(g_3 TT-T2) batch contains 5% of homocoupling of the g_3 TT monomer, which gives rise to a stoichiometric imbalance and thus $r = 0.95$ since both monomers were initially present in equal amounts. We compared the DP predicted by Carothers equation for p after 24 hours in an NMR tube in various DMF-d₇:solvent mixtures (Fig. 3A) and 16 hours in NBP (yield = 97%; Table 1, entry 9) with $M_{n,\text{NMR}}$ from the analysis of high-temperature NMR spectra of the obtained solids after precipitation, which we divided by the weight of the repeat unit $M_{\text{repeat}} = 626.8$ g mol⁻¹ (Fig. 3C, fig. S15, and tables S6 and S7; note that the latter estimate ignores the presence of homocouplings). The obtained values of DP and $M_{n,\text{NMR}}/M_{\text{repeat}}$ are in good agreement, suggesting that the final obtained molecular weights are predominantly determined by the stoichiometric imbalance and conversion, as anticipated given the good solubility of p(g_3 TT-T2) in NBP.

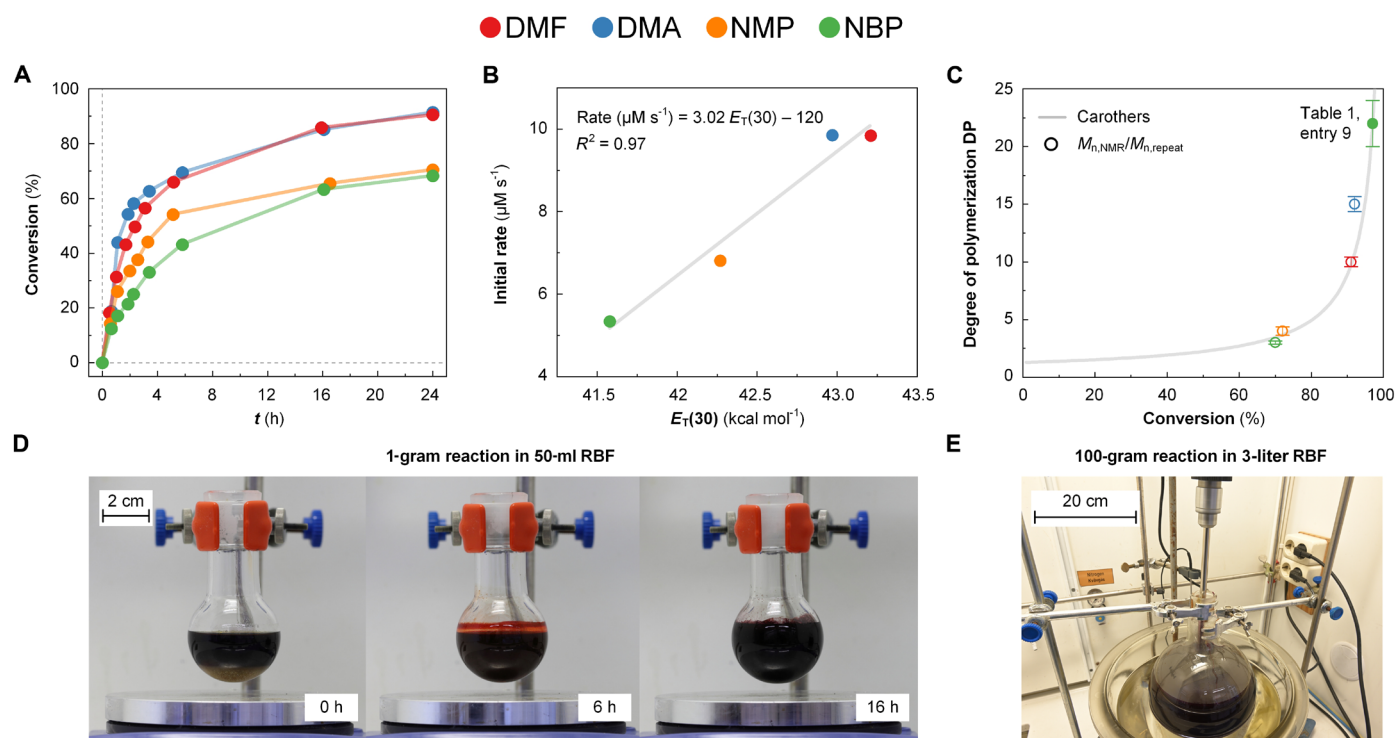


Fig. 3. Kinetics studies and upscaling of ADAP. (A) Reaction progress with respect to time. Conversion determined by NMR using the suppression of the aromatic peak from g_3 TT at 6.79 ppm with respect to the DMF- d_7 peak at 8.03 ppm. (B) Correlation between solvent polarity and rate of reaction. Reichardt's polarity scale defined as the molar absorption energy in kcal mol⁻¹ of Reichardt's betaine B30 dissolved in the relevant solvent (84), using literature values (85). The initial rate corresponds to $dp/dt|_{t=0}$. (C) Correlation between conversion p and degree of polymerization DP of purified polymers compared with Carothers' equation (see Eq. 1). (D) Reaction progress of 1-g scale ADAP in a round-bottom flask (RBF). (E) Photograph of 100-g scale ADAP in a round-bottom flask bearing a mechanical stirrer.

To establish favorable reaction conditions for upscaling and to identify potential limitations regarding the shape of the reaction vessel, we carried out initial 1-g scale experiments in a larger amount of ~25 ml of NBP and used three different reaction vessels: a round-bottom flask, an Erlenmeyer flask, and a beaker. Reaction vessels were left open to air throughout the polymerization, and color changes were recorded (Fig. 3D). We chose to terminate the polymerization after 16 hours because the reaction mixture in the round-bottom and Erlenmeyer flask had adopted a deep purple color, yielding more than 1 g of polymer with an $M_{n,NMR} = 8$ to 9 kg mol⁻¹ (Table 1, entries 10 and 11). Instead, the reaction in the beaker proceeded more slowly, as evidenced by a more magenta color after 16 hours, indicating that the choice of vessel can influence the reaction speed, likely because of differences in convection and hence mixing during the polymerization (fig. S16).

Encouraged by the initial upscaling experiments, we carried out ADAP using 100 g of g_3 TT and 69.8 g of Br-T2-Br in 2.15 liters of NBP. All reagents were added to a one-neck 3-liter round-bottom flask, which was equipped with an overhead mechanical stirrer and suspended in an oil bath set at 25°C. The round-bottom flask was left open to air throughout the polymerization (Fig. 3E). After 30 hours, the reaction mixture was precipitated into *n*-hexanes. The solids were collected, transferred to a Soxhlet thimble, and subsequently purified by extraction with multiple organic solvents (see the Materials and Methods). The chloroform-soluble fraction with $M_{n,NMR} = 11$ kg mol⁻¹ had a total mass of 104 g, equating to a

yield of 76% after workup. The molecular weight of the 1-g batches (Table 1, entries 10 to 12) is lower than the product of small-scale reactions (Table 1, entries 8 and 9) because we deliberately terminated the reaction early to avoid the formation of a higher-molecular weight insoluble fraction. Instead, the 100-g batch (Table 1, entry 13) had a comparable $M_{n,NMR} = 11$ kg mol⁻¹ as small-scale batches (Table 1, entries 8 and 9), indicating that upscaling of the open-flask, room temperature reaction was successful.

ADAP of p(g_3 TT-T2) results in considerable TT-TT homocoupling, compared to almost homocoupling-free polymer prepared by conventional DAP (Table 1, entry 1) (27), which in case of other polymers has led to either less (14, 16, 56) or more (51) ordered materials. We therefore carried out ultraviolet-visible (UV-vis) spectroscopy and grazing incidence wide-angle x-ray scattering (GIWAXS) of p(g_3 TT-T2) made by DAP and ADAP (Table 1, entry 1 versus entries 7 and 9). UV-vis absorption spectra suggest improved order in case of polymers synthesized by ADAP as indicated by the increase in intensity of the peak at 614 nm, which we assign to π -stacking (fig. S43). GIWAXS patterns of ADAP prepared p(g_3 TT-T2) films revealed an edge-on texture as evidenced by strong out-of-plane reflections due to lamellar stacking at $q_{100} = 4.16$ nm⁻¹, $q_{200} = 8.29$ nm⁻¹, and $q_{300} = 12.3$ nm⁻¹, and an in-plane reflection due to π - π stacking at $q_{010} = 16.8$ nm⁻¹ (Fig. 4A and figs. S44 and S45) (27). Both lamellar and π - π stacking reflections were more pronounced compared to p(g_3 TT-T2) synthesized by DAP (Fig. 4A and fig. S46) (27). We argue that the presence of a significant amount of TT-TT homocoupling

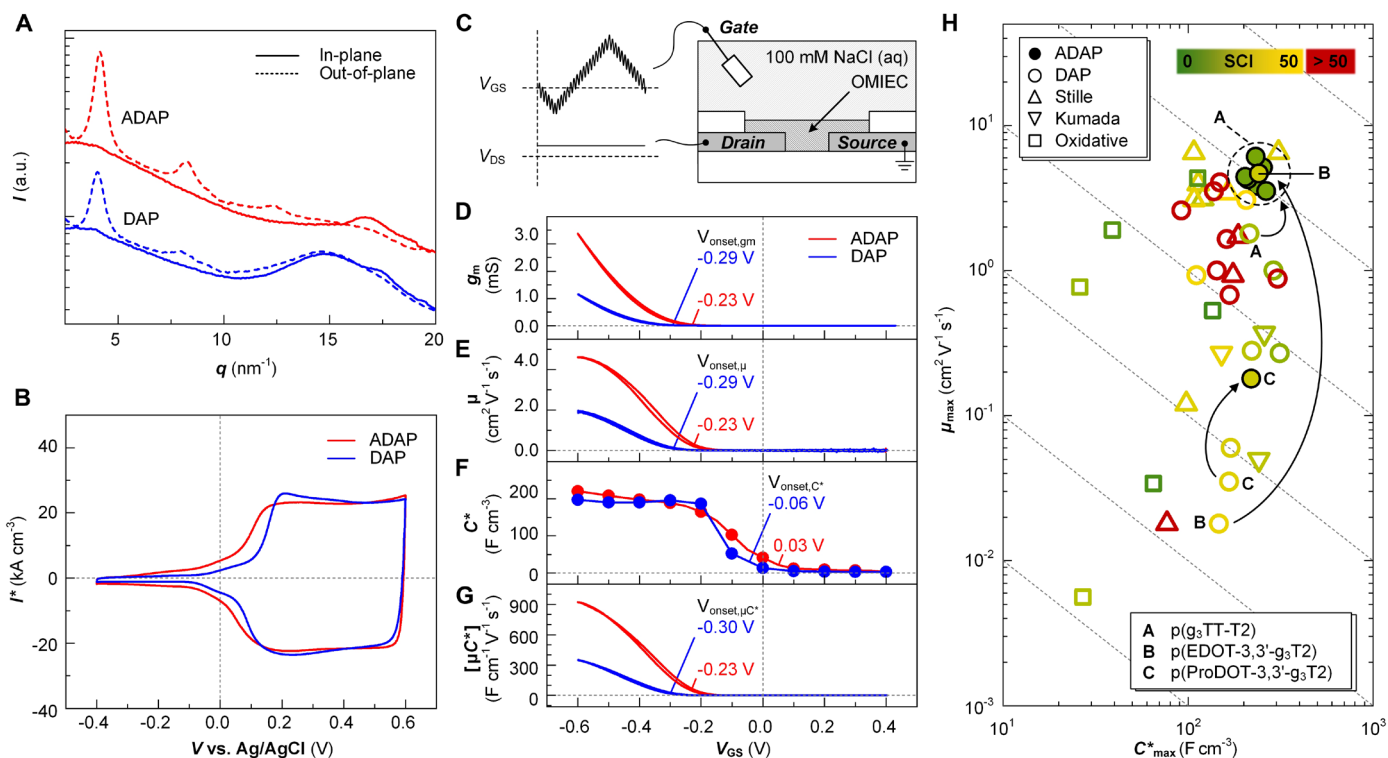


Fig. 4. Nanostructure and electrochemical properties of p(g_3 TT-T2) made by ADAP. (A) In-plane (q_{xy} ; solid lines) and out-of-plane GIWAXS diffractograms (q_z ; dashed lines) of p(g_3 TT-T2) synthesized by ADAP (red) and DAP (blue). (B) Cyclic voltammograms measured in 100 mM NaCl aqueous electrolyte of thin films of p(g_3 TT-T2) synthesized by ADAP (red) and DAP (blue). (C) Device and measurement scheme for small signal analysis. A gate voltage, composed of a triangular waveform combined with a low-amplitude sinusoidal component, is applied to the 100 mM NaCl aqueous electrolyte through a three-electrode system while maintaining a constant drain voltage. Representative traces of (D) transconductance g_m , (E) mobility μ , (F) volumetric capacitance C^* , and (G) the product of mobility and volumetric capacitance $[\mu C^*]$, as a function of V_{GS} obtained by small signal analysis for p(g_3 TT-T2) synthesized by ADAP (red) and DAP (blue). Annotated values correspond to the onset potentials V_{onset} . (H) Ashby plot of maximum volumetric capacitance C^*_{max} and maximum charge-carrier mobility μ_{max} of polymers studied in this work and of previously reported p-type polymers (table S15) (2, 9, 23, 26–29, 63–76). The green-red scale denotes the synthetic complexity index of the full synthesis (SCI_{total}) of starting materials, then monomers, and finally the polymer by ADAP (filled circles), DAP (open circles), Stille coupling (open upward triangles), Kumada coupling (open downward triangles), and oxidative polymerization (open squares). Arrows indicate the improvement that is achieved when changing the polymerization from DAP to ADAP for the three polymers that were used to prepare OECTs: p(g_3 TT-T2), p(EDOT-3,3'- g_3 T2), and p(ProDOT-3,3'- g_3 T2).

resulted in improved order. The high degree of order is attributed to the more rigid nature of homocoupled TT-TT segments, which may promote ordering of adjacent polymer segments, along with the observation that defects lead to smaller chains that can crystallize more easily, as observed for, e.g., poly(3-hexylthiophene) (57–59) and a naphthalene diimide-based copolymer (60).

Cyclic voltammetry was used to determine the oxidation onset energy E_{ox,H_2O} of p(g_3 TT-T2), prepared with ADAP, against Ag/AgCl in 0.1 M NaCl in H₂O (Fig. 4B). E_{ox,H_2O} ranged from 4.42 to 4.57 eV, with a tendency of higher-molecular weight ADAP batches featuring higher values (Table 2). The obtained values were comparable with those measured for p(g_3 TT-T2) prepared with DAP (Table 2) (27).

We fabricated OECT devices to benchmark the electronic performance of p(g_3 TT-T2). Devices comprised gold electrodes with a channel length of 20 μ m and a channel width of 100 μ m, on which patterned films with a thickness of 30 to 60 nm were spin-coated, and an aqueous electrolyte containing 0.1 M NaCl (see Fig. 4C for device layout). The transconductance g_m , μ , C^* , and hence $[\mu C^*]$ were extracted as a function of gate potential V_{GS} , which varied from 0.4 to -0.6 V, with small-signal analysis and electrochemical impedance

spectroscopy [see Materials and Methods and (61) for details]. For example, in case of OECTs based on p(g_3 TT-T2) synthesized in NBP at 25°C (Table 1, entry 9), both g_m and μ increased with decreasing V_{GS} and reached values of $\mu_{max} = 4.4 \text{ cm}^2 \text{ V}^{-1} \text{ s}^{-1}$ at $V_{GS,max} = -0.5 \text{ V}$, where C^* had a value of 204 F cm^{-3} , yielding a figure of merit of $[\mu C^*]_{max} = 899 \text{ F cm}^{-1} \text{ V}^{-1} \text{ s}^{-1}$ (Fig. 4D to G). Overall, we find that μ_{max} ranges from 1.3 to $6.1 \text{ cm}^2 \text{ V}^{-1} \text{ s}^{-1}$, with a tendency for higher values in case of higher-molecular weight batches (Table 2 and figs. S47 to S62). In contrast, p(g_3 TT-T2) made with Ozawa-derived DAP featured a μ_{max} of only $1.9 \text{ cm}^2 \text{ V}^{-1} \text{ s}^{-1}$ despite a high $M_{n,NMR} = 39 \text{ kg mol}^{-1}$ (Table 2). We argue that the superior electrical properties originate from the higher degree of order of ADAP-synthesized p(g_3 TT-T2), which aids electrical transport (62). Concurrently, the onset potential at which the mobility and capacitance increase is shifted to lower V_{GS} by 0.05 to 0.10 V for all ADAP polymers with $M_{n,NMR} > 10 \text{ kg mol}^{-1}$ (Fig. 4D to G, insets).

We compared the here obtained results with literature values for a wide range of polymers prepared by oxidative polymerization, Stille or Kumada cross-coupling, as well as DAP (Fig. 4H, tables S13 to S15, and figs. S63 to S74) (2, 9, 23, 26–29, 63–76). The here prepared p(g_3 TT-T2) batches feature a state-of-the-art OECT performance

Table 2. CV and OECT performance of p(g₃TT-T2). Oxidation onset energy $E_{\text{ox,H}_2\text{O}}$ measured against Ag/AgCl in 0.1 M NaCl in H₂O from -0.4 to 0.6 V; threshold voltage V_{th} obtained from OECT transfer curves; maximum hole mobility μ_{max} obtained through small-signal analysis of OECT devices (67); maximum volumetric capacitance C_{max}^* determined through EIS (one to two samples; error is the max-min value); $[\mu C^*]_{\text{max}}$ obtained by multiplying μ_{max} with C^* at the gate potential $V_{\text{GS,max}}$ where μ_{max} is observed; the mean and SD of the values extracted from n devices are given. The analysis of polymer no. 1 by DAP has been described previously (61).

No.	$E_{\text{ox,H}_2\text{O}}$ (eV)	V_{th} (V)	μ_{max} (cm ² V ⁻¹ s ⁻¹)	C_{max}^* (F cm ⁻³)	$[\mu C^*]_{\text{max}}$ (F cm ⁻¹ V ⁻¹ s ⁻¹)	n
1	4.50 ± 0.003	-0.40 ± 0.002	1.89 ± 0.08	197.3 ± 7.4	432 ± 31	40
2	4.52 ± 0.002	-0.32 ± 0.003	5.14 ± 0.38	254.2 ± 1.1	1006 ± 97.6	14
3	4.51 ± 0.01	-0.32 ± 0.01	6.11 ± 0.38	232.5 ± 4.3	1195 ± 128	13
4	4.45 ± 0.003	-0.25 ± 0.006	3.76 ± 0.60	178 ± 4.0	645 ± 101	4
5	4.50 ± 0.008	-0.24 ± 0.006	2.75 ± 0.30	226.1 ± 0.6	538 ± 57	5
6	4.57 ± 0.0003	-0.36 ± 0.01	3.85 ± 0.26	237.0 ± 3.0	899 ± 49	6
7	4.56	-0.34 ± 0.007	3.53 ± 0.37	264.8	808 ± 130	13
8	4.46 ± 0.002	-0.35 ± 0.002	4.27 ± 0.24	211.2 ± 2.4	963 ± 63	10
9	4.43	-0.36 ± 0.01	4.43 ± 0.19	204 ± 8.0	899 ± 47	15
10	4.43 ± 0.01	-0.36 ± 0.006	1.91 ± 0.12	207.4 ± 1.8	450.4 ± 52.1	5
11	4.42	-0.37 ± 0.002	1.83 ± 0.04	245	370 ± 18.2	5
12	4.42	-0.40 ± 0.004	1.33 ± 0.09	220	212 ± 15	5
13	4.51 ± 0.006	-0.36 ± 0.002	0.96 ± 0.04	230 ± 3.4	269 ± 17	4
14	4.54 ± 0.02*	-0.42 ± 0.05*	1.70 ± 0.20*	224 ± 12*	378 ± 77*	3

*Mean value and max-min error for devices from three different flow batches (see table S12 for mean values and SDs from multiple repeat measurements of devices from each batch).

superior to, e.g., poly(3,4-ethylenedioxythiophene):poly(styrenesulfonate) (PEDOT:PSS) and Stille-polymerized materials such as p(g₃T2-TT). p(g₃TT-T2) prepared by ADAP features a total synthesis SCI that involves not only the polymerization but also the preparation of the monomers (SCI_{total}) as low as 18 (Fig. 4H), which favorably compares with, e.g., p(g₃TT-T2) prepared by DAP (SCI_{total} = 32) (27) and p(g₃T2-TT) prepared by Stille cross-coupling (SCI_{total} = 53) (28), because of a high yield of up to 97% after workup (Table 1, entry 9) and the use of a more benign reaction medium (NBP; Table 1, entries 8 to 13).

In a further set of experiments, we explored to which extent ADAP is a general method that is applicable to other monomer combinations. Pairs of a wide range of H-source and aryl bromide monomers, which are often used for the preparation of OMIECs and are available commercially, were polymerized at room temperature in the presence of Pd(OAc)₂ (Table 3 and figs. S75 to S87) (77). DMA was chosen as the solvent, which resulted in the highest rate of ADAP given the high polarity of the solvent (Fig. 3B). We postulate that the reactions will also proceed in NBP, though at a slower rate, similar to p(g₃TT-T2). Most polymerizations were characterized by a high yield above 70% after workup, with an $M_{\text{n,NMR}} > 10$ kg mol⁻¹ reaching values as high as $M_{\text{n,NMR}} = 34$ kg mol⁻¹ for p(4,4'-g₃T2-T2). Only p(4,4'-g₃T2-TT) led to a low $M_{\text{n,NMR}}$ of 4 kg mol⁻¹, which we assign to the precipitation of the polymer at low temperatures due to its rigid structure (69). ADAP reactions resulted in 3 to 7% H-source homocoupling, which is comparable with p(g₃TT-T2).

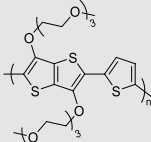
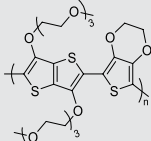
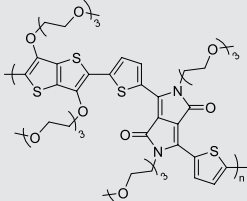
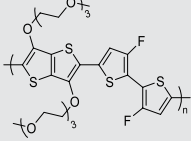
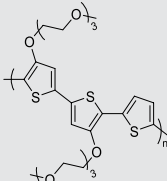
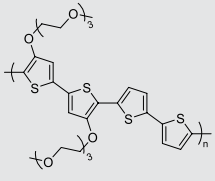
To find out whether the homocoupling generally leads to improved performance, OECTs were fabricated with two other polymers p(EDOT-3,3'-g₃T2) and p(ProDOT-3,3'-g₃T2), both synthesized by ADAP as well as DAP (Fig. 5A, figs. S88 to S92, and table S16). Strikingly, OECTs revealed that the polymers prepared by ADAP featured a significantly higher μ_{max} but similar C^* compared to DAP prepared

materials, yielding a two orders of magnitude higher $\mu_{\text{max}} = 4.6$ cm² V⁻¹ s⁻¹ and thus a high $[\mu C^*]_{\text{max}} = 1112$ F cm⁻¹ V⁻¹ s⁻¹ in case of p(EDOT-3,3'-g₃T2) (Fig. 5B and figs. S88 and S89). We propose that the presence of EDOT or ProDOT homocoupling leads to more rigid segments that encourage the remaining polymer chain segments to order. The increase in order is corroborated by UV-vis spectroscopy, which revealed a red shift in case of ADAP prepared p(EDOT-3,3'-g₃T2) compared to the DAP polymer (Fig. 5A, inset). Accordingly, the onset potential shifted to a lower V_{GS} by ~0.10 V when comparing DAP to ADAP prepared materials, which is indicative of improved electrical transport.

To demonstrate that an even wider range of polymers can be accessed via ADAP, we carried out post-polymerization modification of p(g₃TT-T2F₂). Nucleophilic aromatic substitution (S_NAr) of fluorine bound to the electron-rich thiophene units was readily possible following a protocol inspired by Heeney and colleagues (65, 78). We were able to perform the post-polymerization modification in NBP instead of commonly used chlorobenzene or DMF (65, 78) since p(g₃TT-T2F₂) has high solubility in NBP, especially at elevated temperatures. Modification of p(g₃TT-T2F₂) with a variety of different alcohols and a thiol was evidenced by the distinct change in color of reaction mixtures (more red-purple for apolar functionalization and more purple-blue for polar modification). In addition, the disappearance of the fluorine signal at -125 ppm in high-temperature ¹⁹F NMR spectra indicated near stoichiometric conversion (Fig. 5D and figs. S93 to S98). The final product yield ranged from 67 to 86% after workup, showcasing that ADAP of F-bearing polymers and post-polymerization modification through S_NAr can be readily combined.

Finally, we wanted to improve batch-to-batch reproducibility by translating ADAP to flow synthesis. Attempts to carry out DAP in flow have been met with mixed results because of the long reaction times, which cause, e.g., poor space-time-yield and diffusion that

Table 3. ADAP with different monomer combinations. Reaction conditions: H-source monomer 1.00 equiv, Br-source monomer 1.00 equiv, K_2CO_3 3.00 equiv and $Pd(OAc)_2$ 0.050 equiv in DMA ($[monomer]_0 = 100$ mM) in air at 25°C. Reaction time t , yield from highest molecular weight fraction from Soxhlet extraction relative to the loading of monomers and theoretical yield, and $M_{n,NMR}$ and η_{homo} determined by end group analysis from NMR spectra recorded at 120°C in $C_2D_2Cl_4$.

Polymer (H-source Br-source)	t (hours)	Yield (%)	$M_{n,NMR}$ ($kg\ mol^{-1}$)	η_{homo} (%)
 p(g_3 TT-T)	48*	85	11	4.0
 p(g_3 TT-EDOT)	16	79	25	n.m. [†]
 p(g_3 TT- g_3 DPP)	24	94	12	3.4
 p(g_3 TT-T2F ₂)	24	67	13 [‡]	3.9
 p(g_3 TT-T)	24	74	31	4.4
 p(4,4'- g_3 T2-T)	16	78	33	3.0
 p(4,4'- g_3 T2-T2)				

(Continued)

(Continued)

Polymer (H-source Br-source)	t (hours)	Yield (%)	$M_{n,NMR}$ (kg mol ⁻¹)	n_{homo} (%)
<p>p(4,4'-g₃T₂-TT)</p>	48*	53	4.2	3.3
<p>p(EDOT-3,3'-g₃T₂)</p>	3	89	23	3.9
<p>p(ProDOT-3,3'-g₃T₂)</p>	24	93	20	6.7

*Reaction at 30°C finished in less than 24 hours.

†Not measured due to absence of aromatic protons.

‡ $M_{n,SEC} = 21$ kg mol⁻¹ and PDI = 1.8 (figs. S75 to S87).

interferes with mixing (79). Moreover, the poor solubility of the base in organic solvents necessitates the use of a base-loaded solid-phase reactor that requires cleaning and replenishing of base (42, 43). Since ADAP readily proceeds at room temperature, we anticipated that a fast flow process can be developed provided that a sufficiently high reaction temperature is utilized. A base and solvent combination is required, which is compatible with ADAP and forms a homogeneous mixture. We opted for potassium acetate as the base, which together with all the other reagents readily dissolved in a 9:1 (v/v) binary solvent mixture of NMP and water, thus avoiding the use of a solid-phase reactor altogether. We chose to perform the polymerizations using a droplet flow process, given the potential for a high degree of reproducibility, which is typically achieved using PFAS as a carrier fluid (39, 56). Since the NMP/H₂O solvent mixture is hydrophilic, we were instead able to use silicone oil as a benign carrier fluid given its hydrophobic character. Initial solubility tests between NMP/H₂O and silicone oil revealed no mixing and quick separation of phases following vigorous agitation. The flow setup consisted of four syringe pumps, a reactor equipped with a 2- or 10-ml tube reactor, a backpressure regulator, and a collection vessel with water (Fig. 6A and Materials and Methods). Separate deoxygenated stock solutions of the monomers/base and the catalyst were mixed inside a cross piece. Droplets were created by suspending a small outer

diameter tube, which supplied the reaction mixture in NMP/H₂O, inside a large inner diameter tube, which provided a constant flow of silicone oil. A stable droplet flow was created as was visible in the reactor (Fig. 6A and movie S1). Once the stock solutions were depleted, the reaction mixture was pushed through the reactor using a retention time solvent (here DMF).

We aimed to complete the flow reaction in less than 30 min to achieve a reasonable throughput but also a high degree of control over the polymerization in flow (39, 56, 80). The short reaction time was necessary to maintain effective mixing and avoid unwanted diffusion (81). We attempted ADAP at temperatures ranging from 80° to 140°C with reaction times of 10 to 20 min (Fig. 6B, table S17, and movie S1). All reactions with reaction temperatures ≥100°C had high crude yields. However, polymers synthesized at 100°C were mostly washed away during purification and polymers synthesized at 140°C were largely insoluble. The materials, which showed near 100% yield after purification, were synthesized at 120°C for 15 to 20 min. To assess the reproducibility of the droplet flow reaction, we repeated the reaction at 120°C with a retention time of 20 min. The reaction was performed continuously for 200 min, during which 10 fractions were collected (Tables 1 and 2, entry 14). After purification, with near 100% yield of the active polymer fraction, the 10 fractions showed $M_{n,NMR}$ values of 9 to 13 kg mol⁻¹ (average of $M_{n,NMR} =$

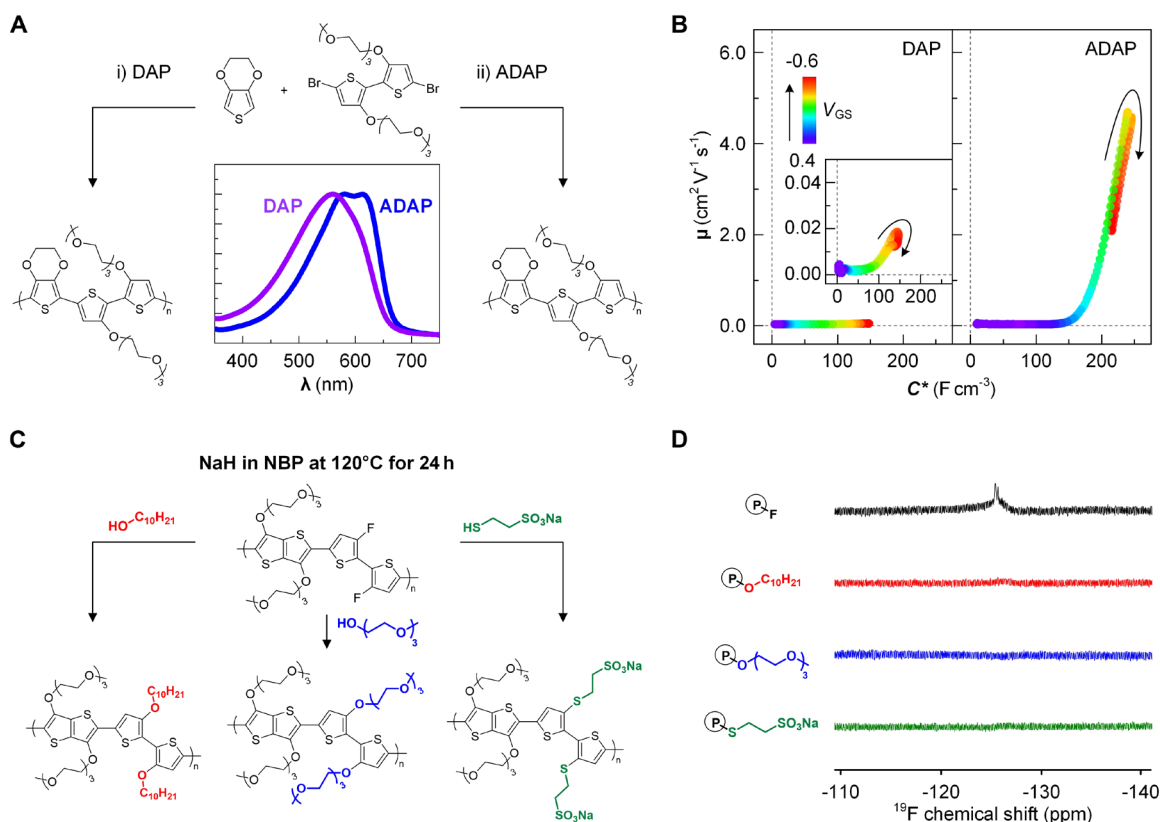


Fig. 5. ADAP with EDOT and post-polymerization functionalization. (A) Synthesis of p(EDOT-3,3'-g₃T₂) by different polymerization methods: (i) DAP using Pd₂dba₃·CHCl₃, P(*o*-anisyl)₃, PivOH, and Cs₂CO₃ in toluene under N₂ at 110°C for 24 hours, and (ii) ADAP using Pd(OAc)₂ and K₂CO₃ in DMA under air at 25°C for 3 hours. The inset showcases normalized solution UV-vis spectra of synthesized polymers in chloroform, and colors indicate the solution colors. (B) OECT μ versus C^* trajectory of p(EDOT-3,3'-g₃T₂) synthesized by DAP (left) and ADAP (right) as a function of V_{GS} . (C) Post-polymerization modification of p(g₃TT-T₂F₂) by nucleophilic aromatic substitution of alcohols and thiol to yield p(g₃TT-T₂alk₂), p(g₃TT-T₂glyc₂), and p(g₃TT-T₂sulf₂). (D) High-temperature ¹⁹F NMR spectra of p(g₃TT-T₂F₂), p(g₃TT-T₂alk₂), p(g₃TT-T₂glyc₂), and p(g₃TT-T₂sulf₂).

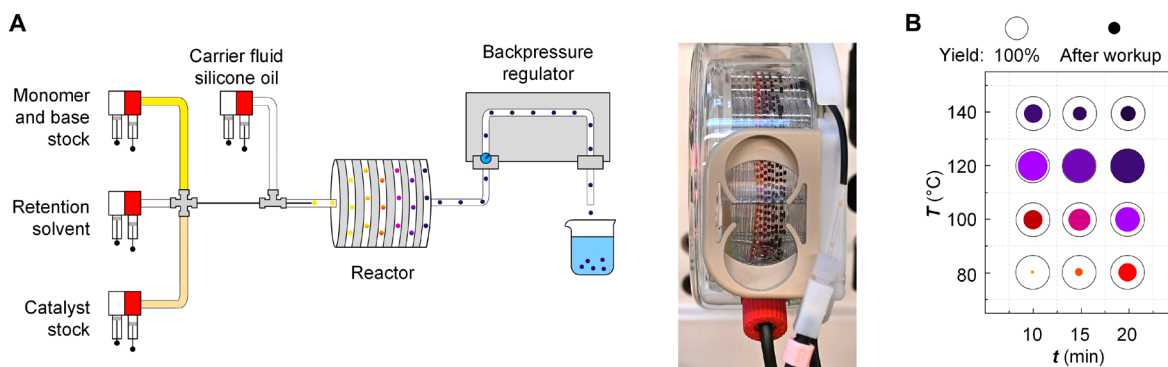


Fig. 6. Translation of polymerization from batch to flow synthesis. (A) Schematic of flow synthesis setup; image to the right showcases NMP/H₂O reaction droplets inside silicone oil in the reactor. (B) Plot showcasing active polymer fraction yields (from chloroform Soxhlet) with respect to reaction time and reaction temperature in the flow setup. The circle border indicates theoretical yield of 100%, and filled circles indicate active polymer fraction yield. Colors indicate the most progressed droplet color in the reactor.

$11 \pm 1 \text{ kg mol}^{-1}$) and homocoupling amounts of $1.5 \pm 0.8\%$, indicative of a highly reproducible flow synthesis process (fig. S41 and tables S9 and S11). We fabricated OECTs from flow-synthesized polymers, which showcased a μ_{max} of $1.7 \pm 0.2 \text{ cm}^2 \text{ V}^{-1} \text{ s}^{-1}$ and C^* of $224 \pm 12 \text{ F cm}^{-3}$, comparable with materials that have a similar molecular weight (Tables 1 and 2, figs. S60 to S62, and table S12).

DISCUSSION

We have introduced ADAP, an efficient approach for the environmentally benign and energy-conscious synthesis of conjugated polymers that is applicable to a wide range of monomer combinations. A further reduction in environmental impact could be achieved by using monomers and solvents derived from natural products and by reducing the number of synthetic steps that are needed to yield the monomer.

Polymerization is made possible by a bimetallic $\text{Pd}^{\text{II}}/\text{Pd}^0$ catalytic system in an amide solvent, which readily proceeds after initiation by homocoupling of an H-source monomer pair. Many previously reported conjugated polymers synthesized by similar Fagnou-derived conditions possibly proceeded by the same mechanism, but this was not considered at the time. By virtue of the spontaneity of the reaction, upscaling of an open-flask, room temperature batch process to over 100 g and translation to highly reproducible continuous flow was possible—the first example of DAP in steady-state droplet flow without the necessity of a solid support and without the need of forever chemicals.

OMIECs synthesized by ADAP comprise homocoupling of the H-source monomer. Contrary to the existing literature, which typically shows that homocoupling results in a decrease in order and hence electronic performance (14, 16, 56), it is observed that polymers prepared by ADAP feature a higher degree of solid-state order compared to polymers without significant homocoupling synthesized by conventional DAP. As a result, the here reported OMIECs feature electrical properties beyond the state of the art, i.e., an OECT mobility μ of up to $6 \text{ cm}^2 \text{ V}^{-1} \text{ s}^{-1}$ and a figure of merit $[\mu C^*] > 1100 \text{ F cm}^{-1} \text{ V}^{-1} \text{ s}^{-1}$. We would like to point out that the increase in μ in case of $\text{p}(\text{ProDOT-3,3}'\text{-g}_3\text{T}_2)$ can be confidently assigned to the homocoupling since the polymers made by DAP and ADAP have comparable molecular weights (20 versus 22 kg mol^{-1}). We argue that the electronic properties of $\text{p}(\text{g}_3\text{TT-T}_2)$ and $\text{p}(\text{EDOT-3,3}'\text{-g}_3\text{T}_2)$ can be improved further by optimizing their molecular weights. While all here investigated polymers that entail homocoupling of the H-source monomer also feature an increase in order, it should not be inferred that homocoupling necessarily leads to improved properties. It is feasible that optimization of the choice of monomer, the amount of homocoupling, and the molecular weight can lead to OMIECs with even better electronic properties, which could possibly be achieved by modifying the bimetallic $\text{Pd}^{\text{II}}/\text{Pd}^0$ catalytic system and by adjusting the monomer ratio (see Carothers equation). Ultimately, it would be interesting to compare perfectly regular polymers with those that feature different amounts of homocoupling of the H-source monomer. We conclude that ADAP is a highly versatile method for the green and large-scale production of conjugated polymers, which is essential for developing truly sustainable organic electronics.

MATERIALS AND METHODS

Chemicals and materials

All solvents including anhydrous and deuterated solvents were obtained from Sigma-Aldrich, Fisher Scientific, or Thermo Fisher Scientific. All reagents and catalysts were obtained from Sigma-Aldrich. Commercially available monomers were purchased from Sigma-Aldrich, TCI, or Ossila. Precursors of monomers g_3TT , $4,4'\text{-g}_3\text{T}_2$, $3,3'\text{-g}_3\text{T}_2\text{Br}_2$, and g_3DPPBr_2 were obtained from Angene, TCI, Sigma-Aldrich, and AA Blocks, respectively. The subsequent monomer syntheses were based on literature procedures (27, 75, 82), which are further described in the Supplementary Materials (previously unrecorded $4,4'\text{-g}_3\text{T}_2$ NMR spectra in figs. S99 and S100).

ADAP in batch

To an appropriate reaction vessel charged with a stirrer bar, the H-source monomer (1.00 equiv), the Br-source monomer (1.00 equiv), potassium carbonate (3.00 equiv), and palladium (II) acetate (0.05 equiv) were added. After addition of the amide solvent ($[\text{monomer}] = 50$ to 100 mM), the reaction vessel was transferred to a heating block (small scale) or oil bath (large scale) set at a temperature of 25°C or left at ambient conditions on a stirrer plate (large scale). In case of small-scale reactions, palladium (II) acetate was added from a stock solution of 2 g liter^{-1} after addition of the corrected amount of amide solvent to the reaction mixture. Reaction progress was monitored by precipitation of aliquots in *n*-hexanes, ethyl acetate, and chloroform, and the reaction was deemed complete when precipitation was observed in ethyl acetate while retaining good solubility in chloroform. After completion, the reaction was precipitated into *n*-hexanes under vigorous stirring. Solids were collected by filtration using qualitative filter paper. Soxhlet extraction was performed with ethyl acetate, and the active fraction was collected using chloroform. This fraction was concentrated in vacuo, and solids were collected and dried.

Post-polymerization modification

A variety of side chains was attached to $\text{p}(\text{g}_3\text{TT-T}_2\text{F}_2)$ by deprotonation of a nucleophile (decan-10-ol, triethylene glycol monomethyl ether, or sodium 2-mercaptoethane-1-sulfonate) in a mixture with NBP using a strong base, followed by the addition of a solution of $\text{p}(\text{g}_3\text{TT-T}_2\text{F}_2)$ in NBP at 40 g liter^{-1} . The reaction was then heated to 120°C for 12 hours. Reaction solvent, the remaining base, and remaining side chains were removed by several precipitations in *n*-hexanes and isopropanol.

Flow setup

Three Syrris Asia syringe pumps were used to hold the monomer/base stock, catalyst stock, and carrier fluid (silicone oil), respectively, and one more Syrris Asia syringe pump was used for the retention time solvent (DMF). The former three pumps were connected to a cross piece with ethylene tetrafluoroethylene (ETFE) tubing [$1/16''$ outer diameter (OD), $0.03''$ inner diameter (ID)]. From the cross piece, the mixed solution was transferred through a T-piece using polyether ether ketone (PEEK) tubing ($1/32''$ OD, $0.02''$ ID), which was held in place until the inlet of the T-piece by using ETFE tubing ($1/16''$ OD, $0.04''$ ID), ETFE tubing ($1/8''$ OD, $0.093''$ ID), and silicone tubing (5 mm OD, 3 mm ID). On the side branch of the same T-piece, the silicone oil pump was connected with ETFE tubing ($1/16''$ OD, $0.03''$ ID). In the outlet of the T-piece, droplets were

generated inside the silicone oil carrier fluid by extending the PEEK tube ($^{1/32}$ " OD, 0.02" ID) with the mixture of monomer/base stock and catalyst stock into a perfluoroalkoxy alkane (PFA) tube ($^{1/16}$ " OD, 0.04" ID). A Vapourtec R4 Reactor Heater/Cooler system equipped with a 2.0- or 10.0-ml standard coiled tube reactor was used for heating the reaction mixture. To provide backpressure, the tubing after the reactor unit was led through a Vapourtec R2 S+ Pumping Module, which was set up as a backpressure regulator. The outlet of the system was suspended over a collection vessel with water. At any connection point (cross piece, T-piece, reactor), tubes were held in place using PEEK nuts and ETFE ferrules matching the respective tubing ODs. Before and after every injection, the system was flushed with DMF.

Polymerization in flow

The monomer/base stock (23.28 g liter⁻¹ g₃TT, 16.22 g liter⁻¹ 5,5'-dibromo-2,2'-bithiophene, and 14.75 g liter⁻¹ potassium acetate) and a separate catalyst stock [1.12 g liter⁻¹ palladium (II) acetate] were prepared using a mixture of NMP and deionized water in a ratio of 9:1. The concentrations of the compounds in their stock solutions were [monomer]:[base]:[catalyst] = 50 mM:150 mM:5.0 mM. Solids were dissolved by heating and sonication. Before loading into the flow system, the stock solutions were left to cool to room temperature, filtered using a syringe filter (0.22 μm pore size), and deoxygenated by argon bubbling for 5 min followed by degassing in an ultrasonic bath for 1 min. Relative flow rates of monomer/base:catalyst:silicone oil were 2:1:3. After the reaction, the mixture was precipitated in a beaker containing deionized water. The collected solids were purified in the same way as the polymers created in batch.

Molecular weight determination with NMR

High-temperature spectra were recorded on an Agilent Technologies 400 MR spectrometer (¹H: 400 MHz). The ¹H NMR spectra were referenced to the residual solvent peak [C₂D₂Cl₄; δ(¹H) = 6.0 ppm]. Characterization of the number-average molecular weight M_n of polymers was performed by end-group analysis from high-temperature spectra in C₂D₂Cl₄ as the deuterated solvent, as described previously (27).

Size exclusion chromatography

Chromatograms were recorded with an Agilent 1260 Infinity GPC at an oven temperature of 70°C. This system utilized two columns and a precolumn containing Polargel M 300 × 7.5 mm, featuring mixed pores with a pore size of 8 μm. Polymer samples were prepared by dissolving them in DMF to a concentration of approximately 1 g liter⁻¹. The eluent consisted of HPLC-grade DMF (Sigma-Aldrich, ≥99.9%) with 0.1 wt % Reagentplus LiBr (Sigma-Aldrich, ≥99.9%). Relative calibration was performed using poly(methyl methacrylate) (PMMA) standards.

Electrochemical characterization

OMIEC films were prepared via spin-coating from a chloroform solution (concentration, 7 to 8 g liter⁻¹) on an indium-doped tin oxide (ITO) coated glass substrate, which was used as the working electrode. Cyclic voltammetry (CV) and electrochemical impedance spectroscopy (EIS) were conducted with 100 mM NaCl aqueous electrolyte with three-electrode configuration (Ag/AgCl reference and Pt counter electrodes) using an SP-300 electrochemical workstation from

BioLogic. Before and during characterization, the electrolyte was purged with nitrogen gas. The oxidation onset energy $E_{\text{ox,H}_2\text{O}}$ was calculated according to $E_{\text{ox,H}_2\text{O}} = -(eV_{\text{onset}} + 4.4 \text{ eV})$, where V_{onset} is the onset oxidation potential versus Ag/AgCl, which was extracted from the x-axis intercept of a linear fit near the maximum slope of the oxidation peak in CV curve. The volumetric capacitance C^* was extracted from EIS data using an equivalent circuit model $R_e [R_s C_s [R_c [R_a C_a]]]$, where R_e , R_s , C_s , R_c , R_a , and C_a are the resistance of the electrolyte, electrochemical resistance/capacitance of the ITO substrate, contact resistance between the substrate and the active layer, and electrochemical resistance/capacitance of the active layer, respectively.

OECT device fabrication

Source and drain metal electrodes were defined via a conventional lift-off process using a Karl Suss MA6 contact aligner and a Kurt J Lesker PVD e-beam evaporator on cleaned Marienfeld soda lime glass slides, resulting in channels with a length $L = 20 \mu\text{m}$. Two parylene films were sequentially deposited with a thickness of 1 and 2 μm with an anti-adhesive soap layer between them. Two parylene films were patterned via a conventional dry-etching process using a Karl Suss MA6 contact aligner and reactive ion etcher (O₂, 300 W), resulting in channel width $w = 100 \mu\text{m}$. Then, a solution of the active layer material (7 to 8 g liter⁻¹ in chloroform) was spin-coated onto the patterned substrate, followed by peeling away of the second parylene film to pattern the active layer. In the case of two polymers (Table 1, entries 4 and 5), active layers were patterned with the parylene-coating and dry-etching process, but partially removed near the contact pads with a swab soaked in chloroform.

OECT device characterization

OECT devices were characterized with a small signal analysis method using a two-channel SP-300 electrochemical workstation from BioLogic, as described previously (61). A mixed gate potential comprising a pseudo-steady-state triangular potential (scan rate = 10 mV s⁻¹) and a sinusoidal AC potential (amplitude = 10 mV, frequency = 10 Hz) was applied through Pt counter and Ag/AgCl reference electrodes using a three-electrode configuration while applying a drain potential of 10 mV. Electrical and electrochemical parameters were calculated with MATLAB software according to (61)

$$G = \frac{I_{\text{DS,DC}}}{V_{\text{DS,DC}}} \quad (2)$$

$$\sigma = \frac{G \cdot L_{\text{ch}}}{wd} \quad (3)$$

$$C^* = \frac{\Delta I''_{\text{GS,AC}}}{2\pi f_{\text{AC}} \Delta V_{\text{GS,AC}} \cdot \text{vol}} \quad (4)$$

$$g_m = \frac{\partial I'_{\text{DS,AC}}}{\partial V_{\text{GS,AC}}} \quad (5)$$

$$\mu = L_{\text{ch}}^2 / \tau_e V_{\text{DS}} \quad (6)$$

where V_{DS} , $I_{\text{DS,DC}}$, and $I'_{\text{DS,AC}}$ are the DC drain voltage, DC drain current, and real component of the AC drain current; $V_{\text{GS,AC}}$ and

$I''_{GS,AC}$ are the AC gate voltage and imaginary component of the AC gate current; τ_e is a transit time obtained according to $\tau_e = -I''_{GS,AC} \cdot (A_{ch}/A_{active}) / (dI'_{DS,AC}/dt)$; and f_{AC} , L_{ch} , w , d , vol , and A_{ch}/A_{active} are the frequency of the applied small signal voltage, channel length, width, thickness of the active layer, volume of the channel layer, and an area correction factor, which is the ratio between the area of the channel region A_{ch} and total active layer A_{active} . The product of mobility and capacitance [μC^*] was obtained by using Eqs. 4 and 6. In case of devices where the parasitic metal line resistance became dominant due to a very high mobility (Table 1 and 2, entries 2, 3, and 6 to 9), the parasitic resistance values were corrected by using the measured line resistance value of each channel (details are given in the Supplementary Materials) (83). Alternatively, OECTs were characterized with two MATLAB-controlled Keithley 2400 source-measure units (Table 1 and 2, entries 4 and 5). The gate potential was applied through an Ag/AgCl reference electrode and a Pt counter electrode, using a three-electrode configuration. The drain-source potential was applied using a two-electrode configuration.

Supplementary Materials

The PDF file includes:

Supplementary Text
Figs. S1 to S100
Tables S1 to S17
Legend for movie S1
References

Other Supplementary Material for this manuscript includes the following:

Movie S1

REFERENCES AND NOTES

- M. Craighero, Q. Li, Z. Zeng, C. Choi, Y. Kim, H. Yoon, T. Liu, P. Sowinski, S. Haraguchi, B. Hwang, B. Mihiretie, S. Fabiano, C. Müller, Poly(benzodifurandione) coated silk yarn for thermoelectric textiles. *Adv. Sci.* **11**, 2406770 (2024).
- A. Giovannitti, C. B. Nielsen, D.-T. Sbircea, S. Inal, M. Donahue, M. R. Niazi, D. A. Hanifi, A. Amassian, G. G. Malliaras, J. Rivnay, I. McCulloch, N-type organic electrochemical transistors with stability in water. *Nat. Commun.* **7**, 13066 (2016).
- Y. He, N. A. Kukhta, A. Marks, C. K. Luscombe, The effect of side chain engineering on conjugated polymers in organic electrochemical transistors for bioelectronic applications. *J. Mater. Chem. C* **10**, 2314–2332 (2022).
- D. Kiefer, A. Giovannitti, H. Sun, T. Biskup, A. Hofmann, M. Koopmans, C. Cendra, S. Weber, L. J. Anton Koster, E. Olsson, J. Rivnay, S. Fabiano, I. McCulloch, C. Müller, Enhanced n-doping efficiency of a naphthalenediimide-based copolymer through polar side chains for organic thermoelectrics. *ACS Energy Lett.* **3**, 278–285 (2018).
- D. Moia, A. Giovannitti, A. A. Szumska, I. P. Maria, E. Rezasoltani, M. Sachs, M. Schnurr, P. R. F. Barnes, I. McCulloch, J. Nelson, Design and evaluation of conjugated polymers with polar side chains as electrode materials for electrochemical energy storage in aqueous electrolytes. *Energy Environ. Sci.* **12**, 1349–1357 (2019).
- J. Kuwabara, T. Kanbara, “2—Green synthetic approaches to π -conjugated polymers for thin-film transistors and photovoltaic application” in *Sustainable Strategies in Organic Electronics*, A. Marrocchi, Ed. (Woodhead Publishing, 2022), chap. 2, pp. 75–94.
- I. McCulloch, M. Chabincyn, C. Brabec, C. B. Nielsen, S. E. Watkins, Sustainability considerations for organic electronic products. *Nat. Mater.* **22**, 1304–1310 (2023).
- Y. Wang, E. Zeglio, L. Wang, S. Cong, G. Zhu, H. Liao, J. Duan, Y. Zhou, Z. Li, D. Mawad, A. Herland, W. Yue, I. McCulloch, Green synthesis of lactone-based conjugated polymers for n-type organic electrochemical transistors. *Adv. Funct. Mater.* **32**, 2111439 (2022).
- R. Po, G. Bianchi, C. Carbonera, A. Pellegrino, “All that glitters is not gold”: An analysis of the synthetic complexity of efficient polymer donors for polymer solar cells. *Macromolecules* **48**, 453–461 (2015).
- R. A. Sheldon, The E factor at 30: A passion for pollution prevention. *Green Chem.* **25**, 1704–1728 (2023).
- A. P. Dicks, A. Hent, “Atom economy and reaction mass efficiency” in *Green Chemistry Metrics: A Guide to Determining and Evaluating Process Greenness*, A. P. Dicks, A. Hent, Eds. (Springer International Publishing, 2015), chap. 2, pp. 17–44.
- S. Broll, F. Nübling, A. Luzio, D. Lentzas, H. Komber, M. Caironi, M. Sommer, Defect analysis of high electron mobility diketopyrrolopyrrole copolymers made by direct arylation polycondensation. *Macromolecules* **48**, 7481–7488 (2015).
- F. Lombeck, H. Komber, S. I. Gorelsky, M. Sommer, Identifying homocouplings as critical side reactions in direct arylation polycondensation. *ACS Macro Lett.* **3**, 819–823 (2014).
- J. Vanderspikken, Z. Liu, X. Wu, O. Beckers, S. Moro, T. J. Quill, Q. Liu, A. Goossens, A. Marks, K. Weaver, M. Hamid, B. Goderis, E. Nies, V. Lemaire, D. Beljonne, A. Salleo, L. Lutsen, K. Vandewal, B. Van Mele, G. Costantini, N. Van den Brande, W. Maes, On the importance of chemical precision in organic electronics: Fullerene intercalation in perfectly alternating conjugated polymers. *Adv. Funct. Mater.* **33**, 2309403 (2023).
- A. E. Rudenko, B. C. Thompson, Optimization of direct arylation polymerization (DARp) through the identification and control of defects in polymer structure. *J. Polym. Sci. A Polym. Chem.* **53**, 135–147 (2015).
- M. Streiter, D. Beer, F. Meier, C. Göhler, C. Lienert, F. Lombeck, M. Sommer, C. Deibel, Homocoupling defects in a conjugated polymer limit exciton diffusion. *Adv. Funct. Mater.* **29**, 1903936 (2019).
- K. H. Hendriks, W. Li, G. H. L. Heintges, G. W. P. van Pruijsen, M. M. Wienk, R. A. J. Janssen, Homocoupling defects in diketopyrrolopyrrole-based copolymers and their effect on photovoltaic performance. *J. Am. Chem. Soc.* **136**, 11128–11133 (2014).
- A. L. Mayhugh, P. Yadav, C. K. Luscombe, Circular discovery in small molecule and conjugated polymer synthetic methodology. *J. Am. Chem. Soc.* **144**, 6123–6135 (2022).
- R. Matsidik, H. Komber, A. Luzio, M. Caironi, M. Sommer, Defect-free naphthalene diimide bithiophene copolymers with controlled molar mass and high performance via direct arylation polycondensation. *J. Am. Chem. Soc.* **137**, 6705–6711 (2015).
- Q. Wang, R. Takita, Y. Kikuzaki, F. Ozawa, Palladium-catalyzed dehydrohalogenative polycondensation of 2-bromo-3-hexylthiophene: An efficient approach to head-to-tail poly(3-hexylthiophene). *J. Am. Chem. Soc.* **132**, 11420–11421 (2010).
- N. Zhou, A. S. Dudnik, T. I. N. G. Li, E. F. Manley, T. J. Aldrich, P. Guo, H.-C. Liao, Z. Chen, L. X. Chen, R. P. H. Chang, A. Facchetti, M. Olvera de la Cruz, T. J. Marks, All-polymer solar cell performance optimized via systematic molecular weight tuning of both donor and acceptor polymers. *J. Am. Chem. Soc.* **138**, 1240–1251 (2016).
- S. T. M. Tan, A. Gumyusenge, T. J. Quill, G. S. LeCroy, G. E. Bonacchini, I. Denti, A. Salleo, Mixed ionic–electronic conduction, a multifunctional property in organic conductors. *Adv. Mater.* **34**, e2110406 (2022).
- S. Inal, G. G. Malliaras, J. Rivnay, Benchmarking organic mixed conductors for transistors. *Nat. Commun.* **8**, 1767 (2017).
- A. L. Jones, M. De Keersmaecker, L. R. Savagian, B. T. DiTullio, I. Pelse, J. R. Reynolds, Branched oligo(ether) side chains: A path to enhanced processability and elevated conductivity for polymeric semiconductors. *Adv. Funct. Mater.* **31**, 2102688 (2021).
- J. F. Ponder Jr., A. M. Österholm, J. R. Reynolds, Conjugated polyelectrolytes as water processable precursors to aqueous compatible redox active polymers for diverse applications: Electrochromism, charge storage, and biocompatible organic electronics. *Chem. Mater.* **29**, 4385–4392 (2017).
- B. Ding, V. Le, H. Yu, G. Wu, A. V. Marsh, E. Gutiérrez-Fernández, N. Ramos, M. Rimmle, J. Martín, J. Nelson, A. F. Paterson, M. Heeney, Development of synthetically accessible glycolated polythiophenes for high-performance organic electrochemical transistors. *Adv. Electron. Mater.* **10**, 2300580 (2024).
- J. Kimpel, Y. Kim, J. Asatryan, J. Martin, R. Kroon, C. Müller, High-mobility organic mixed conductors with a low synthetic complexity index via direct arylation polymerization. *Chem. Sci.* **15**, 7679–7688 (2024).
- A. Giovannitti, D.-T. Sbircea, S. Inal, C. B. Nielsen, E. Bandiello, D. A. Hanifi, M. Sessolo, G. G. Malliaras, I. McCulloch, J. Rivnay, Controlling the mode of operation of organic transistors through side-chain engineering. *Proc. Natl. Acad. Sci. USA* **113**, 12017–12022 (2016).
- S. Griggs, A. Marks, D. Meli, G. Rebetez, O. Bardagot, B. D. Paulsen, H. Chen, K. Weaver, M. I. Nugraha, E. A. Schafer, J. Tropp, C. M. Aitchison, T. D. Anthopoulos, N. Banerji, J. Rivnay, I. McCulloch, The effect of residual palladium on the performance of organic electrochemical transistors. *Nat. Commun.* **13**, 7964 (2022).
- B. Ma, Q. Shi, X. Ma, Y. Li, H. Chen, K. Wen, R. Zhao, F. Zhang, Y. Lin, Z. Wang, H. Huang, Defect-free alternating conjugated polymers enabled by room-temperature stille polymerization. *Angew. Chem. Int. Ed. Engl.* **61**, e202115969 (2022).
- H. Xiong, Q. Lin, Y. Lu, D. Zheng, Y. Li, S. Wang, W. Xie, C. Li, X. Zhang, Y. Lin, Z.-X. Wang, Q. Shi, T. J. Marks, H. Huang, General room-temperature Suzuki–Miyaura polymerization for organic electronics. *Nat. Mater.* **23**, 695–702 (2024).
- A. Bakry, P. Yadav, S.-Y. Chen, C. K. Luscombe, The unexpected fast polymerization during the synthesis of a glycolated polythiophene. *Faraday Discuss.* **250**, 74–82 (2024).
- A. L. Mayhugh, C. K. Luscombe, Room-temperature Pd/Ag direct arylation enabled by a radical pathway. *Beilstein J. Org. Chem.* **16**, 384–390 (2020).
- G. E. Castillo, B. C. Thompson, Room temperature synthesis of a well-defined conjugated polymer using direct arylation polymerization (DARp). *ACS Macro Lett.* **12**, 1339–1344 (2023).

35. H. Seyler, D. J. Jones, A. B. Holmes, W. W. H. Wong, Continuous flow synthesis of conjugated polymers. *Chem. Commun.* **48**, 1598–1600 (2012).
36. H. Seyler, J. Subbiah, D. J. Jones, A. B. Holmes, W. W. H. Wong, Controlled synthesis of poly(3-hexylthiophene) in continuous flow. *Beilstein J. Org. Chem.* **9**, 1492–1500 (2013).
37. J. H. Bannock, M. J. Heeney, J. C. de Mello, "Flow synthesis: A better way to conjugated polymers?" in *Conjugated Polymers: Perspective, Theory, and New Materials* (CRC Press, ed. 4, 2019), chap. 16, pp. 613–652.
38. J. H. Bannock, S. H. Krishnasadan, A. M. Nightingale, C. P. Yau, K. Khaw, D. Burkitt, J. J. M. Halls, M. Heeney, J. C. de Mello, Continuous synthesis of device-grade semiconducting polymers in droplet-based microreactors. *Adv. Funct. Mater.* **23**, 2123–2129 (2013).
39. O. Beckers, S. Gielen, F. Verstraeten, P. Verstappen, L. Lutsen, K. Vandewal, W. Maes, Continuous droplet flow synthesis of a near-infrared responsive push–pull copolymer toward large scale implementation of organic photodetectors. *ACS Appl. Polym. Mater.* **2**, 4373–4378 (2020).
40. M. Heeney, J. C. de Mello, A reflection on 'Controlled synthesis of conjugated random copolymers in a droplet-based microreactor'. *Materials Horizons* **12**, 668–672 (2025).
41. M. G. Evich, M. J. B. Davis, J. P. McCord, B. Acrey, J. A. Awkerman, D. R. U. Knappe, A. B. Lindstrom, T. F. Speth, C. Tebes-Stevens, M. J. Strynar, Z. Wang, E. J. Weber, W. M. Henderson, J. W. Washington, Per- and polyfluoroalkyl substances in the environment. *Science* **375**, eabg9065 (2022).
42. N. S. Gobalasingham, J. E. Carlé, F. C. Krebs, B. C. Thompson, E. Bundgaard, M. Helgesen, Conjugated polymers via direct arylation polymerization in continuous flow: Minimizing the cost and batch-to-batch variations for high-throughput energy conversion. *Macromol. Rapid Commun.* **38**, 1700526 (2017).
43. F. Grenier, B. R. Aïch, Y.-Y. Lai, M. Guérette, A. B. Holmes, Y. Tao, W. W. H. Wong, M. Leclerc, Electroactive and photoactive poly[isindigo-alt-edot] synthesized using direct (hetero) arylation polymerization in batch and in continuous flow. *Chem. Mater.* **27**, 2137–2143 (2015).
44. J. Lopez, S. Pletscher, A. Aemissegger, C. Bucher, F. Gallou, N-butylpyrrolidinone as alternative solvent for solid-phase peptide synthesis. *Org. Process Res. Dev.* **22**, 494–503 (2018).
45. L.-C. Campeau, K. Fagnou, Palladium-catalyzed direct arylation of simple arenes in synthesis of biaryl molecules. *Chem. Commun.* **1253–1264**, (2006).
46. D. Kim, G. Choi, W. Kim, D. Kim, Y. K. Kang, S. H. Hong, The site-selectivity and mechanism of Pd-catalyzed C(sp²)-H arylation of simple arenes. *Chem. Sci.* **12**, 363–373 (2021).
47. J. Kuwabara, M. Sakai, Q. Zhang, T. Kanbara, Mechanistic studies and optimisation of a Pd-catalysed direct arylation reaction using phosphine-free systems. *Org. Chem. Front.* **2**, 520–525 (2015).
48. J. Kim, S. H. Hong, Ligand-promoted direct C–H arylation of simple arenes: Evidence for a cooperative bimetallic mechanism. *ACS Catal.* **7**, 3336–3343 (2017).
49. D. Adamczak, H. Komber, A. Illy, A. D. Scaccabarozzi, M. Caironi, M. Sommer, Indacenodithiophene homopolymers via direct arylation: Direct polycondensation versus polymer analogous reaction pathways. *Macromolecules* **52**, 7251–7259 (2019).
50. H. Zhao, C.-Y. Liu, S.-C. Luo, B. Zhu, T.-H. Wang, H.-F. Hsu, H. H. Yu, Facile syntheses of dioxithiophene-based conjugated polymers by direct C–H arylation. *Macromolecules* **45**, 7783–7790 (2012).
51. A. L. Jones, M. De Keersmaecker, I. Pelse, J. R. Reynolds, Curious Case of BiEDOT: MALDI-TOF mass spectrometry reveals unbalanced monomer incorporation with direct (Hetero) arylation Polymerization. *Macromolecules* **53**, 7253–7262 (2020).
52. N. S. Gobalasingham, B. C. Thompson, Direct arylation polymerization: A guide to optimal conditions for effective conjugated polymers. *Prog. Polym. Sci.* **83**, 135–201 (2018).
53. W. A. Carole, T. J. Colacot, Understanding palladium acetate from a user perspective. *Chem. A Eur. J.* **22**, 7686–7695 (2016).
54. C. Carlucci, D. Conelli, O. Hassan Omar, N. Margiotta, R. Grisorio, G. P. Suranna, Toward eco-friendly protocols: Insights into direct arylation polymerizations under aerobic conditions in anisole. *Polym. Chem.* **14**, 343–351 (2023).
55. R. M. Pankow, L. Ye, N. S. Gobalasingham, N. Salami, S. Samal, B. C. Thompson, Investigation of green and sustainable solvents for direct arylation polymerization (DARp). *Polym. Chem.* **9**, 3885–3892 (2018).
56. S. Smeets, Q. Liu, J. Vanderspikken, T. J. Quill, S. Gielen, L. Lutsen, K. Vandewal, W. Maes, Structurally pure and reproducible polymer materials for high-performance organic solar cells. *Chem. Mater.* **35**, 8158–8169 (2023).
57. A. G. Dixon, R. Visvanathan, N. A. Clark, N. Stingelin, N. Kopidakis, S. E. Shaheen, Molecular weight dependence of carrier mobility and recombination rate in neat P3HT films. *J. Polym. Sci. B Polym. Phys.* **56**, 31–35 (2018).
58. F. P. V. Koch, J. Rivnay, S. Foster, C. Müller, J. M. Downing, E. Buchaca-Domingo, P. Westacott, L. Yu, M. Yuan, M. Baklar, Z. Fei, C. Luscombe, M. A. McLachlan, M. Heeney, G. Rumbles, C. Silva, A. Salleo, J. Nelson, P. Smith, N. Stingelin, The impact of molecular weight on microstructure and charge transport in semicrystalline polymer semiconductors–poly(3-hexylthiophene), a model study. *Prog. Polym. Sci.* **38**, 1978–1989 (2013).
59. P. Kohn, S. Huettner, H. Komber, V. Senkovskyy, R. Tkachov, A. Kiriy, R. H. Friend, U. Steiner, W. T. S. Huck, J.-U. Sommer, M. Sommer, On the role of single regiodefects and polydispersity in regioregular Poly(3-hexylthiophene): Defect distribution, synthesis of defect-free chains, and a simple model for the determination of crystallinity. *J. Am. Chem. Soc.* **134**, 4790–4805 (2012).
60. M. M. Nahid, R. Matsidik, A. Welford, E. Gann, L. Thomsen, M. Sommer, C. R. McNeill, Unconventional molecular weight dependence of charge transport in the high mobility n-type semiconducting polymer P(NDI2OD-T2). *Adv. Funct. Mater.* **27**, 1604744 (2017).
61. Y. Kim, J. Kimpel, A. Giovannitti, C. Müller, Small signal analysis for the characterization of organic electrochemical transistors. *Nat. Commun.* **15**, 7606 (2024).
62. R. Noriega, J. Rivnay, K. Vandewal, F. P. V. Koch, N. Stingelin, P. Smith, M. F. Toney, A. Salleo, A general relationship between disorder, aggregation and charge transport in conjugated polymers. *Nat. Mater.* **12**, 1038–1044 (2013).
63. O. Bardagot, B. T. DiTullio, A. L. Jones, J. Speregin, J. R. Reynolds, N. Banerji, Balancing electroactive backbone and oligo(ethylene oxy) side-chain content improves stability and performance of soluble pedot copolymers in organic electrochemical transistors. *Adv. Funct. Mater.* **35**, 2412554 (2025).
64. I.-Y. Jo, D. Jeong, Y. Moon, D. Lee, S. Lee, J.-G. Choi, D. Nam, J. H. Kim, J. Cho, S. Cho, D.-Y. Kim, H. Ahn, B. J. Kim, M.-H. Yoon, High-performance organic electrochemical transistors achieved by optimizing structural and energetic ordering of diketopyrrolopyrrole-based polymers. *Adv. Mater.* **36**, e2307402 (2024).
65. B. Ding, I.-Y. Jo, H. Yu, J. H. Kim, A. V. Marsh, E. Gutiérrez-Fernández, N. Ramos, C. L. Rapley, M. Rimmel, Q. He, J. Martin, N. Gasparini, J. Nelson, M.-H. Yoon, M. Heeney, Enhanced organic electrochemical transistor performance of donor–acceptor conjugated polymers modified with hybrid glycol/ionic side chains by postpolymerization modification. *Chem. Mater.* **35**, 3290–3299 (2023).
66. B. Ding, G. Kim, Y. Kim, F. D. Eisner, E. Gutiérrez-Fernández, J. Martin, M.-H. Yoon, M. Heeney, Influence of backbone curvature on the organic electrochemical transistor performance of glycolated donor–acceptor conjugated polymers. *Angew. Chem. Int. Ed.* **60**, 19679–19684 (2021).
67. L. Q. Flagg, C. G. Bischak, J. W. Onorato, R. B. Rashid, C. K. Luscombe, D. S. Ginger, Polymer crystallinity controls water uptake in glycol side-chain polymer organic electrochemical transistors. *J. Am. Chem. Soc.* **141**, 4345–4354 (2019).
68. R. Halaksa, J. H. Kim, K. J. Thorley, P. A. Gilhooly-Finn, H. Ahn, A. Savva, M.-H. Yoon, C. B. Nielsen, The influence of regiochemistry on the performance of organic mixed ionic and electronic conductors. *Angew. Chem. Int. Ed.* **62**, e202304390 (2023).
69. R. K. Hallani, B. D. Paulsen, A. J. Petty II, R. Sheelamanthula, M. Moser, K. J. Thorley, W. Sohn, R. B. Rashid, A. Savva, S. Moro, J. P. Parker, O. Drury, M. Alsufyani, M. Neophytou, J. Kosco, S. Inal, G. Costantini, J. Rivnay, I. McCulloch, Regiochemistry-driven organic electrochemical transistor performance enhancement in ethylene glycol-functionalized polythiophenes. *J. Am. Chem. Soc.* **143**, 11007–11018 (2021).
70. D. G. Harman, R. Gorkin, L. Stevens, B. Thompson, K. Wagner, B. Weng, J. H. Y. Chung, M. I. H. Panhuis, G. G. Wallace, Poly(3,4-ethylenedioxythiophene):dextran sulfate (PEDOT:DS) – A highly processable conductive organic biopolymer. *Acta Biomater.* **14**, 33–42 (2015).
71. S.-M. Kim, C.-H. Kim, Y. Kim, N. Kim, W.-J. Lee, E.-H. Lee, D. Kim, S. Park, K. Lee, J. Rivnay, M.-H. Yoon, Influence of PEDOT:PSS crystallinity and composition on electrochemical transistor performance and long-term stability. *Nat. Commun.* **9**, 3858 (2018).
72. L. Lindell, A. Burquel, F. L. E. Jakobsson, V. Lemaire, M. Berggren, R. Lazzaroni, J. Cornil, W. R. Salaneck, X. Crispin, Transparent, Plastic, Low-Work-Function Poly(3,4-ethylenedioxythiophene) Electrodes. *Chem. Mater.* **18**, 4246–4252 (2006).
73. X. Luo, H. Shen, K. Perera, D. T. Tran, B. W. Boudouris, J. Mei, Designing donor–acceptor copolymers for stable and high-performance organic electrochemical transistors. *ACS Macro Lett.* **10**, 1061–1067 (2021).
74. M. Moser, T. C. Hidalgo, J. Surgailis, J. Gladisch, S. Ghosh, R. Sheelamanthula, Q. Thiburce, A. Giovannitti, A. Salleo, N. Gasparini, A. Wadsworth, I. Zozoulenko, M. Berggren, E. Stavrinidou, S. Inal, I. McCulloch, Side chain redistribution as a strategy to boost organic electrochemical transistor performance and stability. *Adv. Mater.* **32**, e2002748 (2020).
75. C. B. Nielsen, A. Giovannitti, D.-T. Sbircea, E. Bandiello, M. R. Niazi, D. A. Hanifi, M. Sessolo, A. Amassian, G. G. Malliaras, J. Rivnay, I. McCulloch, Molecular design of semiconducting polymers for high-performance organic electrochemical transistors. *J. Am. Chem. Soc.* **138**, 10252–10259 (2016).
76. J. W. Onorato, Z. Wang, Y. Sun, C. Nowak, L. Q. Flagg, R. Li, B. X. Dong, L. J. Richter, F. A. Escobedo, P. F. Nealey, S. N. Patel, C. K. Luscombe, Side chain engineering control of mixed conduction in oligoethylene glycol-substituted polythiophenes. *J. Mater. Chem. A* **9**, 21410–21423 (2021).
77. J. Tropp, D. Meli, J. Rivnay, Organic mixed conductors for electrochemical transistors. *Matter* **6**, 3132–3164 (2023).
78. A. Creamer, C. S. Wood, P. D. Howes, A. Casey, S. Cong, A. V. Marsh, R. Godin, J. Panidi, T. D. Anthopoulos, C. H. Burgess, T. Wu, Z. Fei, I. Hamilton, M. A. McLachlan, M. M. Stevens, M. Heeney, Post-polymerisation functionalisation of conjugated polymer backbones and its application in multi-functional emissive nanoparticles. *Nat. Commun.* **9**, 3237 (2018).

79. A. K. Coker, "Chapter Eight—Residence time distributions in flow reactors" in *Modeling of Chemical Kinetics and Reactor Design* (Gulf Professional Publishing, 2001), chap. 8, pp. 663–761.
80. B. Zhang, A. Mathoor, T. Junkers, High throughput multidimensional kinetic screening in continuous flow reactors. *Angew. Chem. Int. Ed. Engl.* **62**, e202308838 (2023).
81. C. A. Hone, C. O. Kappe, Towards the standardization of flow chemistry protocols for organic reactions. *Chem. Methods* **1**, 454–467 (2021).
82. A. Punzi, F. Nicoletta, G. Marzano, C. G. Fortuna, J. Dagar, T. M. Brown, G. M. Farinola, Synthetic routes to teg-substituted diketopyrrolopyrrole-based low band-gap polymers. *Eur. J. Org. Chem.* **2016**, 3233–3242 (2016).
83. M. J. Donahue, A. Williamson, X. Strakosas, J. T. Friedlein, R. R. McLeod, H. Gleskova, G. G. Malliaras, High-performance vertical organic electrochemical transistors. *Adv. Mater.* **30**, 1705031 (2018).
84. C. Reichardt, Solvatochromic dyes as solvent polarity indicators. *Chem. Rev.* **94**, 2319–2358 (1994).
85. J. Sherwood, H. L. Parker, K. Moonen, T. J. Farmer, A. J. Hunt, N-Butylpyrrolidinone as a dipolar aprotic solvent for organic synthesis. *Green Chem.* **18**, 3990–3996 (2016).
86. M. J. Dávila, J. P. Martin Trusler, Thermodynamic properties of mixtures of N-methyl-2-pyrrolidinone and methanol at temperatures between 298.15K and 343.15K and pressures up to 60MPa. *J. Chem. Thermodyn.* **41**, 35–45 (2009).
87. J. P. E. Grolier, G. Roux-Desgranges, M. Berkane, E. Jiménez, E. Wilhelm, Heat capacities and densities of mixtures of very polar substances 2. Mixtures containing N, N-dimethylformamide. *J. Chem. Thermodyn.* **25**, 41–50 (1993).
88. I. Shehatta, Heat capacity at constant pressure of some halogen compounds. *Thermochim. Acta* **213**, 1–10 (1993).
89. T. H. Syed, T. J. Hughes, K. N. Marsh, E. F. May, Isobaric heat capacity measurements of liquid methane, ethane, and propane by differential scanning calorimetry at high pressures and low temperatures. *J. Chem. Eng. Data* **57**, 3573–3580 (2012).
90. Overview of materials for low alloy steel. MatWeb Material Property Data. <https://www.matweb.com/search/datasheet.aspx?matguid=d1bdbccde4da4a4a9dbb8918d783b29&n=1> [accessed 25 November 2024].
91. Ş. Ç. Yener, T. Yener, R. Mutlu, Convection coefficient estimation of still air using an infrared thermometer and curve-fitting. *J. Eng. Appl. Sci. Technol.* **4**, 95–103 (2019).

Acknowledgments: We thank R. Matsidik for performing MALDI-TOF measurements, J. Heimonen for assistance with SEC measurements, and R. Xiong for assistance with high-temperature NMR. This project made use of the NMR Uppsala infrastructure, which is funded by the Department of Chemistry—BMC and the Disciplinary Domain of Medicine and Pharmacy, Uppsala University. The Swedish NMR Centre at the University of Gothenburg is acknowledged for its support. Myfab is acknowledged for support and access to the nanofabrication laboratory at Chalmers. **Funding:** J.K., D.R.H., M.S., and C.M. gratefully acknowledge financial support from the European Union's Horizon 2020 research and innovation programme through the Marie Skłodowska-Curie grant agreement no. 955837 (HORATES). Y.K. and C.M. gratefully acknowledge financial support from the Knut and Alice Wallenberg Foundation (grant agreement nos. 2021.0295 and 2022.0034) and the European Research Council (ERC) under grant agreement no. 101043417. R.K. acknowledges support by the Wallenberg Initiative Materials Science for Sustainability (WISE) funded by the Knut and Alice Wallenberg Foundation. **Author contributions:** J.K. and C.M. conceptualized the study, visualized the data, and wrote the original draft. J.K., Y.K., H.S., D.H., J.A., J.M., R.K., M.S., and C.M. reviewed and edited the draft. J.K. performed all synthetic procedures and chemical characterization with associated method development, investigation, analysis, and validation. D.H. further investigated and validated the synthetic procedures. R.K. and M.S. provided access to the SEC and NMR, respectively, and contributed to supervision of synthesis. Y.K. performed all OECT measurements with associated software programming, method development, investigation, analysis, and validation. H.S. provided access to the flow system and LC-MS, and performed the necessary method development and investigation. J.A. and J.M. carried out GIWAXS with associated method development, investigation, and analysis. J.M. provided access to the synchrotron and supervised GIWAXS measurements. J.K. and Y.K. collected and deposited all data in a data repository. R.K., M.S., and C.M. acquired funding for the study. C.M. provided resources throughout, analyzed results, and supervised the overall study. **Competing interests:** H.S. is a co-founder and chief technology officer of AutoSyn AB. All other authors declare no competing interests. **Data and materials availability:** All data needed to evaluate the conclusions in the paper are present in the paper and/or the Supplementary Materials. Additional data can be accessed via DOI: 10.5281/zenodo.15111531.

Submitted 8 January 2025

Accepted 1 April 2025

Published 7 May 2025

10.1126/sciadv.adv8168